# Study of the reflective properties of *Tyvek* used in water Cherenkov detectors at the *Pierre Auger Observatory*

# Untersuchung der Reflexionseigenschaften von *Tyvek* in Wasser-Cherenkov-Detektoren am *Pierre Auger Observatorium*

Bachelor Thesis
zur Erlangung des akademischen Grades
*Bachelor of Science*

dem Fachbereich Physik
der Bergischen Universität Wuppertal

vorgelegt von
**Alex Kääpä**

15.07.2013

Betreuender Professor:    Prof. Dr. Karl-Heinz Kampert
Zweitkorrektor:              Prof. Dr. Christian Zeitnitz

Acknowledgements

It is impossible to portray the gratitude I have in a way, which actually expresses how indebted I feel to those people, who accompanied and supported me during the completion of this thesis. Therefore, the order, with which I name these people, in no way should be viewed as an order, with which I value their contributions.

I will start off with thanking *Karl-Heinz Kampert*, my supervising professor, i.a. for supporting me in finding a suitable topic, for organising all the necessary paperwork for getting the application of the thesis swiftly done, helping me find a second corrector, namely *Christian Zeitnitz* − whom I also want to thank for agreeing to assume this role − , and giving me suggestions for possible experiments. A lot of unnecessary waste of time was spared, which was especially convenient considering the short time you have writing a Bachelor's Thesis.

The biggest technical support was given by *Sven Querchfeld*, who gave me the necessary background to the status quo of the research on the topic and to the possible experimental setups, and who discussed my findings with me, guiding the way to think about them. For all this I am very grateful. Thanks goes also to *Julian Rautenberg*, who organised the weekly meetings with the Auger group of our university, in which we discussed our research sofar, which helped me organise myself during this time. I also want to thank him for looking into my latest results, as time was running out, and relieved me from some of the stress which started boiling up. Both Sven's and Julian's technical suggestions after proofreading also came in very handy.

The support provided by *Uwe Naumann* and *Djahangir Pouryamput*, especially in preparing parts for setups and overseeing me when operating more or less heavy machinery, as well as helpful suggestions from *Christian Pauly*, were also very much appreciated. I am also grateful to *Andreas Tepe* for lending me his camera, and *Nicole Krohm*, *Carla Bleve* and *Sasche Reinecke* for their technical assistance.

Though not directly contributing to the topic of the thesis, I have to thank *Philipp Papenbreer* for helping during data analysis, especially in getting to know *ROOT*. The casual, but not work impeding atmosphere in the office I worked in also helped me during the work on my thesis, for which I want to thank Philipp and my other office colleagues *Jens Neuser* and *Lukas Niemitz*. *Ms. Schaarwächter* also deserves thanks for helping me complete different kinds of paperwork, though not related to this thesis.

As I was measuring for and writing my thesis mid-semester, the work load at times became rather high. Therefore, I feel very indebted to *Sabrina Hintz*, *Katrin Jonuleit*, *Jörg Förtsch*, *Christina Ballnus* and *Teodora Nikolova* for taking some of it off my back.

My thesis would have been a lot more difficult to complete without moral support from friends and family, especially my parents *Pia* and *Olli* for showing interest and support, and my brother *Niko*, for reminding me of the value of balancing the work with some amount of leisure time.

At last, I want to show my deepest gratitude to *Lisa*, who assisted me in a multitude of ways during the past three months, showed unwavering support, patience and kindness, and helped me carry my burden more than anyone else.

## Abstract

In this thesis, reflectivity measurements are performed on *DuPont*™ *Tyvek*®, which is used in the liners of water-Cherenkov detectors at the *Pierre Auger Observatory*, the largest earthbound experiment designed to measure ultra-high energy cosmic rays ($E \geq 10^{18}$ eV). Its purpose is to reflect Cherenkov light, emitted by high-energy particles as they enter the water tank. Throughout the years, the detector's performance has decreased; a contributing factor is a changing *Tyvek* reflectivity. Therefore, comparative measurements between samples, which had been used in the water tanks, and unused ones, are of main importance. Experiments covered are diffuse reflectivity measurements with the *integrating sphere*, specular reflectivity measurements with the so-called *reflection probe* and angular distribution measurements to determine the proportion of the two above components. In addition, structural differences between used and unused samples with the scanning electron microscope, the effects of freezing *Tyvek*, and the hypothesis that *nano bubbles* attach on its fibres when immersed in water which eventually dissipate, are studied.

All measurements are constrained by the high inhomogeneity of *Tyvek*, thus they carry large measurement uncertainties and have limited significance. Still, it shows that used *Tyvek* has a lower diffuse and specular reflectivity than unused *Tyvek*. The angular distribution measurements show no detectable difference in the proportion of these components, although a measurement series with the reflection probe suggests a slightly higher diffuse component. The SEM scans show that macroscopic structural differences between used and unused *Tyvek* (wrinkles and black "spots"on the used sample) has no microscopic origins, and most likely merely result from different fibre densities. Freezing *Tyvek* has no measurable effects on its reflectivity. Evidence of the existence of nano bubbles was found: The reflectivity of *Tyvek* decreases with time of it being immersed in water and seems to converge towards a final value, and the decrease is consistent with measured data from the detector performance; in addition, treating *Tyvek* in an ultrasonic bath, which is thought to detach the bubbles from the surface, also leads to a decreased reflectivity in a similar manner, although some observations suggest that the decrease could in part be due to a damage of the *Tyvek*.

## Zusammenfassung

Im Rahmen dieser Arbeit werden Reflektivitätsmessungen an *DuPont*™ *Tyvek*® durchgeführt, welches sich im Innenmantel der Wasser-Cherenkov-Detektors des *Pierre Auger Observatorium*s, dem weltweitgrößten Experiment zur Messung ultra-hochenergetischer kosmischer Strahlung ($E \geq 10^{18}$ eV), befindet. Das *Tyvek* dient dabei der Reflexion von Cherenkov-Strahlung, welche hochenergetische Teilchen beim Eindringen in die Wasser-Tanks emittieren. In den Jahren seit Inbetriebnahme haben die Detektoren an Leistungsfähigkeit verloren, was unter anderem auf eine veränderte Reflektivität des *Tyvek* zurückgeführt werden kann. Daher sind Vergleichsmessungen zwischen Proben, welche in den Wasser-Tanks eingebaut waren, und unbenutzen Proben, von besonderer Bedeutung. Darunter fallen diffuse Reflektivitätsmessungen mit der *Ulbricht-Kugel*, gerichtete Reflexionsmessungen mit der sogenannten *Reflection Probe* und Messungen der winkelabhängigen Verteilung von an *Tyvek* reflektiertem Licht, die dem Vergleich des relativen Anteils der eben erwähnten Komponenten von der Gesamtreflektivität zwischen den Proben dienen. Außerdem werden strukturelle Unterscheide zwischen den Probentypen mit einem Rasterelektronenmikroskop, der Einfluss des Einfrierens von *Tyvek*, und die Hypothese, dass sich *Nano-Bläschen* beim Eintauchen von *Tyvek* in Wasser an den Fasern bilden, untersucht.

Alle Messreihen tragen wegen der großen Inhomogenität von *Tyvek* große Messunsicherheit mit sich und haben daher eine eingeschränkte Aussagekraft. Nichtsdestotrotz stellt sich heraus, dass benutztes *Tyvek* sowohl eine geringere diffuse als auch gerichtete Reflektivität als unbenutztes *Tyvek* aufweist. Messungen der winkelabhängigen Verteilung von reflektierter Strahlung zeigen keinen messbaren Unterschied zwischen beiden Proben, eine Messreihe mit der Reflection Probe weist jedoch auch einen geringfügig höheren gerichteten Anteil bei unbenutzem *Tyvek* auf. Die Rasterelektronenmikroskopaufnahmen zeigen, dass beobachtete makroskopische strukturelle Unterschiede zwischen benutztem und unbenutztem *Tyvek* (Knicke und schwarze Flecken an benutzten Proben) keinen mikroskopischen Ursprung haben, und höchstwahrscheinlich von einer unterschiedlichen Faserdichte herrühren. Das Einfrieren von *Tyvek* hat keine messbaren Auswirkungen auf seine Reflektivität. Es gibt Hinweise auf die Existenz von Nano-Bläschen: Die Reflektivität von *Tyvek* nimmt mit der Zeit, die es in Wasser eingetaucht ist, ab und strebt einem Grenzwert entgegen, und die Abnahme ist verträglich mit Messdaten aus den Wasser-Detektoren; des Weiteren verringert die Behandlung von *Tyvek* mit einem Ultraschallbad, welches die Bläschen von der Oberfläche lösen soll, die Reflektivität auf ähnliche Weise, obwohl einige Beobachtungen vermuten lassen das die Abnahme zum Teil einer Beschädigung des *Tyvek* geschuldet ist.

# Contents

# Chapter 1

# Introduction and motivation of thesis

Over a hundred years ago, in 1912, *Viktor Hess* (1883 - 1964) conducted his historic balloon-borne experiment, in which he sought to obtain information on the source of the ionising radiation which had been discovered less than two decades before. At that time it was believed that the radiation originated from the earth, thus he expected to measure a decreasing flux with increasing altitude of the balloon. Yet − after an initial decrease − he measured the complete opposite, leading him to the conclusion that the radiation must have an extraterrestrial source. He coined the word "*Höhenstrahlung*" (German for "*altitude radiation*") to describe this radiation, today the term *cosmic rays* (CR) is primarily used [1].

Since then, extensive research has been done on cosmic rays, yielding evermore insight into its origins. In 2008, the *Pierre Auger Observatory* (PAO) in Argentina, the largest earthbound experiment for measuring cosmic rays comprising 1660 surface detectors (water-Cherenkov detectors; abbrevitation: SD) and 27 fluorescence detectors (radio telescopes; abbreviation: FD) distributed among four sites, covering an area of 3000 km$^2$, was deployed and has been collecting data with unequalled precision eversince. Several new discoveries have been made, especially concerning the directional correlation of incoming cosmic rays [1].

Needless to say, in order to ensure an optimal collection of data, especially of ultra high-energy cosmic rays (UHECR) ($E > 10^{19}$eV) and to enable quantitative measurements of different parameters, such as the mass and energy of the particles constituting the cosmic rays, the properties of the detectors have to optimally monitored and understood. Within the scope of this thesis, I will focus on the surface detectors, more exactly the tank liner, which consists inter alia of *DuPont*$^{\text{TM}}$ *Tyvek*®, a white flashspun fabric made of fibres of polyethylene [2]. Its primary function is to reflect Cherenkov light, which is produced in the tank, onto the photo-mutiplier tubes (PMT) at the top of the liner.

In the course of the 5 years, during which the experiment at the PAO has been running, and beyond (some SDs had already been operational as early as 2004, the SD performance has shown ageing effects, which are best visible in an increased dip-to-hump ratio of the charge histograms by approximately 15 %, and in a decreased muon decay time and area over peak (AoP) ratio by approximately the same amount (these quantities will be elucidated in chapter 2). Possible factors, which could influence the performance, are the water quality in the tank, on the one hand, and the change of overall reflectivity of the *Tyvek*, on the other.

There are two observations made from the above data, which are insofar special as their occurrence correlates (temporally) with events, which were taking place at the SDs at that time: The first is a sharp decrease of the AoP during a period, when the temperatures at the site was below zero, and the water in the tanks began to freeze; the second is a jump in the AoP at the time, when the water was refilled in a particular SD, followed by a gradual decrease back to its previous value. It is to be noted, that the signal never reaches the same value it had, when the detectors were first put into operation. Both observations reinforce the assumption, that the reflectivity of *Tyvek* has been changing over the years: On the one hand, freezing water will not change the water quality, but can very well damage the fibres in the *Tyvek*, which would lead to a lower reflectivity. On the other hand, the fact that the AoP never reaches the initial value from the time, that the detector was put into operation, even after exchanging the water and thus, maximising its

quality again, strongly implies a decreased reflectivity. In addition, there is a hypothesis to explain the progress of the AoP after exchanging the water, namely that microscopic air bubbles, which will be called *nano bubbles*, could develop when immersing *Tyvek* in water, which gradually dissipate.

Lastly, when removed from the tank and directly examined, several changes in the macroscopic structure of the *Tyvek* are visible: The fibre density has significantly decreased, leaving several black "spots" on the surface and several kinks can be seen in the fabric, which do not turn up in unused specimen.

The main objective of my thesis, therefore, will be to measure the reflective properties of *Tyvek*. In particular I will compare these properties between two types of samples, those, which had been used in the liners of the SDs and being subject to the above described phenomena, and those that had not. Further goals will be to investigate the influence of freezing *Tyvek*. Whether the structural changes, which were observed in the used *Tyvek* samples, for example the "spots", have microscopic origins, will also be studied.

The structure of the thesis will be as follows: In chapter 2, some theoretical background will be given in order to provide the necessary framework and background for the thesis. Topics discussed will be cosmic rays, the PAO and its SDs, the properties of *Tyvek*, both with regards to the SDs and independently of them, and the theory of the integrating sphere. In chapter 3 to 6 the different experiments, with which the structural and reflective properties of *Tyvek* were measured, are presented and discussed. Chapter 3 focuses on microscopic changes in the *Tyvek*'s structure after having been used in the SDs, chapter 4 is devoted to the diffuse reflectivity (explanation in chapter 2 section 4), chapter 5 to the specular reflectivity, and chapter 6 to the measurement of both.

# Chapter 2

# Theoretical background

In the thesis, experimental setups and materials (i.e. the *Tyvek*) will be used, which require somewhat specific background knowledge of the reader. Therefore, the theoretical framework for several topics need to be discussed. First of all, an introduction to cosmic rays and to the *Pierre Auger Observatory* with the main focus on the surface detectors will be given. When speaking about the SDs, the role *Tyvek* plays will be illustrated. In addition, *Tyvek*'s properties, separately from its function for the PAO, will be outlined. Lastly, *Lambert's cosine law*, which describes the radiant intensity of diffusely reflecting surfaces (such as *Tyvek*) will be discussed, together with the theoretical background of the integrating sphere.

## 2.1   Cosmic Rays and the *Pierre Auger Observatory*

First evidence of the existence of cosmic radiation was given by *Viktor Hess*, as has already been mentioned in the introduction of this thesis (chapter 1). In several balloon-borne experiments, mountain expeditions and satellite measurements, vast amounts of information concerning this radiation have been obtained. Today, several facts about its energy, composition and origins are known and will be presented in the following. As reference I will use [3].

Cosmic radiation is extraterrestrial, mostly ionising, radiation, consisting of different kinds of particles. It is mainly composed of charged particles, such as protons ($\approx 83$ %), but also of heavier atomic nuclei, all the way up to iron ($\approx 12$ % for $\alpha$-particles and $\approx 3$ % for particles with $Z \geq 3$). Its energy ranges from about $10^8$ eV to about $10^{20}$ eV (see figure 2.1 a)), extending over 12 orders of magnitude and with highest energies far exceeding the energies modern particle accelerators are capable of producing. Thus, investigation in the physics of UHECR is of importance already insofar as it uniquely reveals information of yet untested realms, of the high-energy processes taking place within and outside our galaxy, which can accelerate particles to such energies.

When these high-energy particles, called *primary cosmic rays*, enter the earth's atmosphere, they interact with atmospheric particles. The interaction products further interact with the atmosphere, producing ever more *secondary particles* at ever higher rates causing a so-called *extensive air shower* (EAS; see figure 2.1 b)). Depending on energy and kind of cosmic particle responsible for the first interaction, the structure, composition and distribution of the shower varies. By measuring the shower and reconstructing its path, information about the primary particles can be drawn.

With increasing energy of the particles, the flux decreases by 31 orders of magnitude, spanning a range from 1000 per second and square metre to 1 per century and square kilometre (see figure 2.1 a)). In effect, experiments comprising ever larger areas are needed for measuring ultra high-energy particles with adequate precision within a reasonable period of time. While high-altitude experiments would be able to gather more direct information about the particles, they become increasingly unviable with their limited size for measuring the small flux at higher energies, therefore one is forced to confine oneself to earthbound experiments.

a)

b)
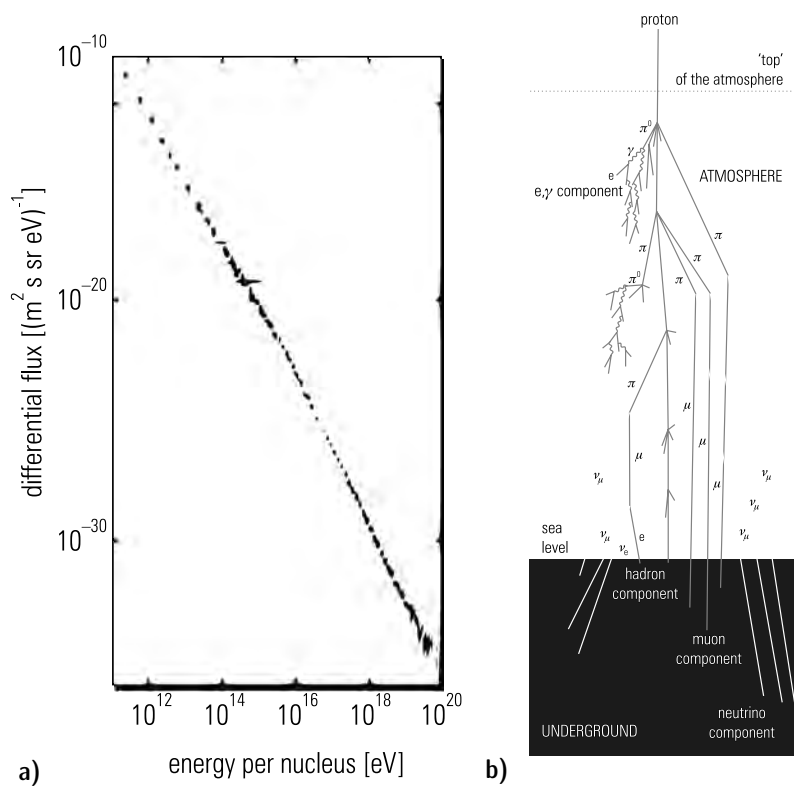
Figure 2.1: a) Energy spectrum of all particles constituting primary cosmic rays; b) Illustration of an air shower (From: [3]

The biggest experiment of this kind is the *Pierre Auger Observatory* (PAO), situated in the western Argentinian plain called *Pampa Amarilla* (see figure 2.2). It is named after the physicist *Pierre Auger* (1899 - 1993), who is credited with the discovery of extensive air showers. As mentioned in the introduction, the PAO makes use of two detections methods: The first is measuring incoming high-energy particles through the measurement of Cherenkov radiation, which they emit as they travel through water with a higher velocity than the speed of light in that medium. This is done in 1660 water tanks spanning an area of 3000 km$^2$. The second method is the detection of fluorescence radiation as a result of the particles interacting with atmospheric nitrogen, done with 27 radio telescopes. Both combined make up a so-called "hybrid detector", which complement each other in such a way as to allow the data acquisition to occur with unequalled precision.
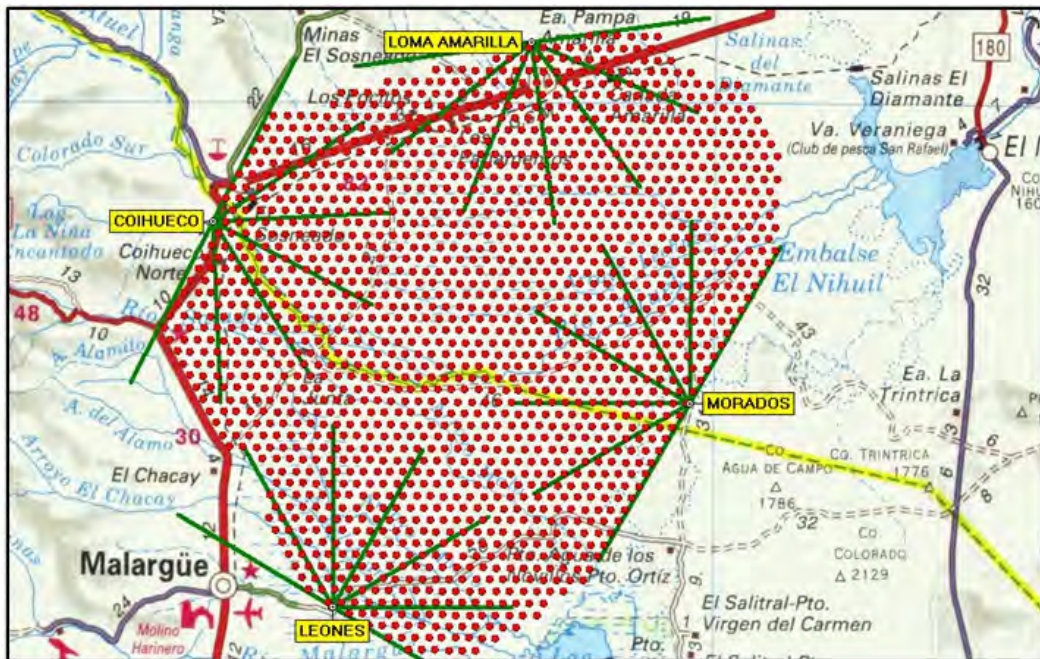


Figure 2.2: Bird's-eye view of the PAO site; the red dots depict the positions of the SD tanks and the four points from which the green lines spread radially give the sites of the FD telescopes (From: Auger south website [4])

As has also been stated in the introduction, the water-Cherenkov detectors are of special interest for this thesis, as the *Tyvek*, which is to be analysed, is an integral part in the liner of the tank.

## 2.2   Surface detectors

For the description of the SD tanks I will refer to [6] and [7]. The basic structure of the surface detectors is depicted in figure 2.3. It consists of a rotationally moulded polyethylene tank, 3.6 m in diameter and 1.55 m in height, comprising a volume of 12,000 L of highly purified water. At the top 3 PMTs are mounted facing the water through windows which are set into the top surface of the liner. An electronic box containing the front-end electronics for digitalisation of the PMT signals is mounted at an aerial on top of the tank, providing radio communication between the surface detectors. Power is provided by solar panels and stored in batteries.
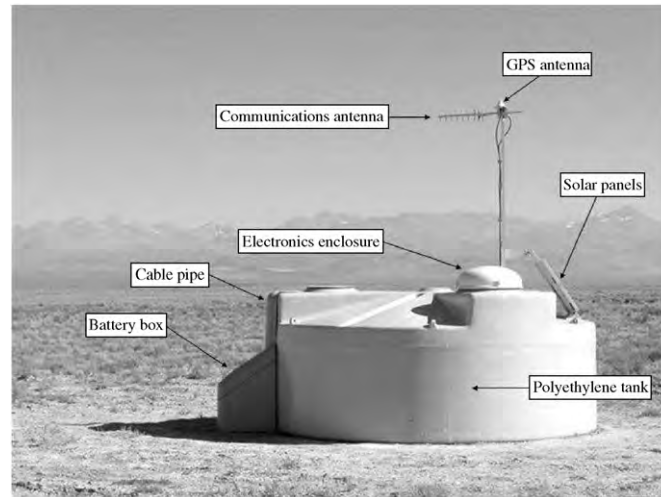


Figure 2.3: a) Photograph of the SD(From: [5])

I will now focus on the liner of the tank. It also has a cylindrical shape designed to contain the entire volume of water. Its laminate is made of several layers of polyolefin plastics. The inner layer is a 140 μm thick sheet of the *Tyvek*, the others consist of polyethylene films (see 2.4). While the outer layers are designed to shield the inside from external light and to keep the water inside the liner, the *Tyvek* performs the liner's key task of reflecting the Cherenkov radiation onto the PMTs and thereby providing a higher signal.
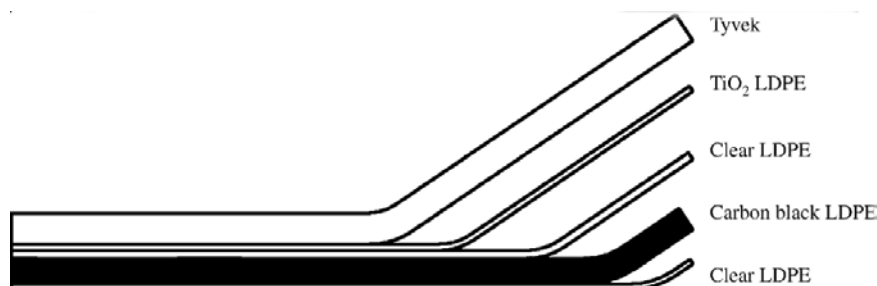


Figure 2.4: Sketch of the laminate of the liner depicting the different layers (From: [6])

As has been alluded to in the introduction of this thesis, the SDs have been showing some ageing effects in the course of the 9 years they have been operational. This has become most apparent in the change of their performance, which I will illustrate on the basis of three quantities: the muon decay time, the charge histograms and the AoP ratio. My references will be [7], [8], [9], [10], [11], [12] and [13].

For purposes of context I will first introduce the *vertical equivalent muon* (VEM). It plays a large role in the calibration of the surface detectors and in the measurement of the amount of energy deposited in a single SD.

A VEM is the average charge produced in a PMT by a vertical and centrally through-going muon (VCT) via Cherenkov radiation. In figure 2.5 the simulated charge histogramm (i.e. the charge distribution) of 1000 VCT muons is depicted. The peak of the plot, namely the charge deposited by most muons, is called the VEM peak, and the area, which is also the total charge deposited, is called the VEM area. The actual VEM is not depicted in the plot, but is given by the VEM area divided by the number of muons.
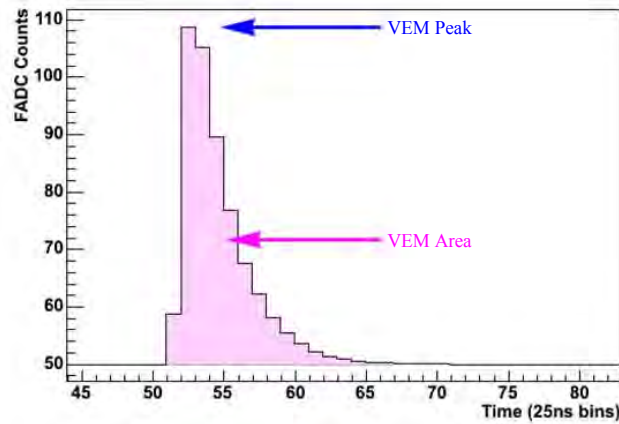


Figure 2.5: Simulated charge histogram from 1000 VCT muons (From: [8])

In the calibration process, each recorded signal is converted into units of VEM. This conversion is done in order to have a common reference point for each SD, or to calibrate against detector simulations for further Monte Carlo (MC) studies [7].

The VEM is inferred from charge histograms of atmospheric or background muons. Unlike VCT muons, they need not enter the SDs vertically, or centrally. As a result, the track length of atmospheric muons in the SDs is not equal to its height, but continuously distributed. The signal correlates linearly with the track length distribution [9], thus, the charge distribution of the PMTs is different from that of VCT muons shown in figure 2.5. In figure 2.6, the background muon charge histogram collected by all three PMTs in an SD, together with the actual VEM, can be seen. Two peaks are visible for atmospheric muons, yet only the second peak is of interest, as the appearance of the first is due to a low trigger threshold which allows for the contribution of short-tracked muons (those decaying inside the tank, as well as those with inclined clipped tracks) and other particles, such as photons and electrons. There are two visible differences between the spectra, namely a shift of the peak to about 1.09 VEM [7] and a longer tail for the one from background muons. Note that the linear relationship of signal and track length is only given if the light in the tanks is fully isotropic and has large attenuation lengths. This only applies for the total signal collected by all the PMTs; for single PMTs, the light in the tank is dependent on the entry point of the particle [9] and the single-PMT signal would peak at $(1.03 \pm 0.03)$ VEM [7].

With regards to energy deposit, the VEM Area, namely the total charge deposited by VCT muons, is a direct unit of measure of this very quantity. This area is subject to both short and long term changes. While those of short term, mainly fluctuations with cycle durations in the order of days, are well understood and considered in the calibration of the detectors, changes over longer periods of time have only been sparsely examined. An area decrease over a longer period of time (far exceeding four hours) by the factor of 2 would not be problematic, but if this decrease amounted a factor of 10, the effects could not be corrected for [8].

The VEM area and, thus, the VEM itself are strongly affected by the reflectivity of the *Tyvek* in the liner of the SD, as can be seen in figure 2.7. To track the changes of the reflective properties of the *Tyvek* the so-called area-over-peak ratio (AoP ratio) is used, which is the ratio between the VEM area and the VEM peak. Although figure 2.7 shows the dependence of the so-called muon decay constant, which is the signal decay time, the AOP is used as a proxy because it is basically affected by the same parametres (a change in *Tyvek* reflectivity mostly affects the signal from multiple reflections and thus decreases the VEM area, while the peak is largely unaffected, and thereby also the AoP ratio), while being more constrained than the decay constant, and thus easier to measure [8].

7
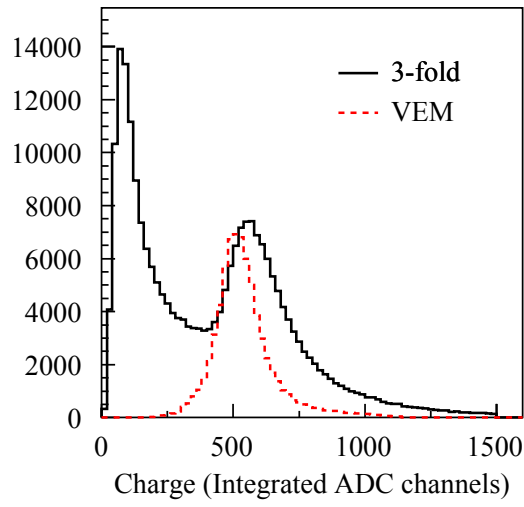
Figure 2.6: Charge histogram (black) and the VEM (pink) (From: [7]
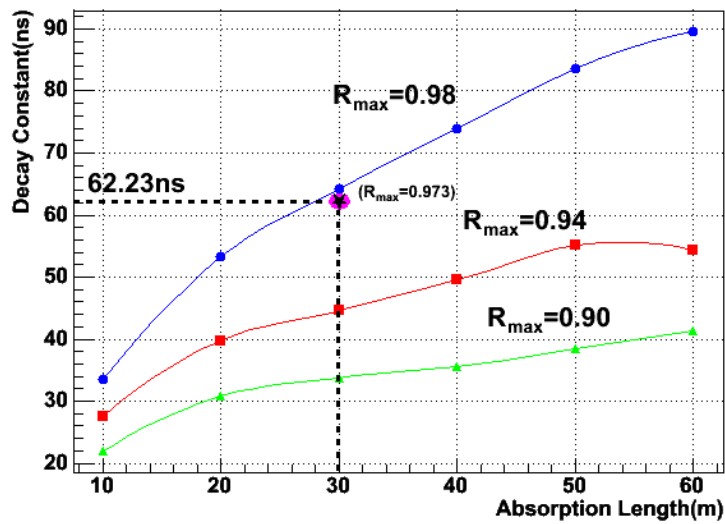


Figure 2.7: Dependence of the muon decay constant on the reflectivity of *Tyvek* (From: [8])

Another quantity affected by changing *Tyvek* reflectivity is the dip-to-hump ratio of the atmospheric muon charge histograms, i.e. the ratio between the height of the dip between the two peaks and the height of the second peak. The dip is heavily dependent on the amount of noise, i.e. the short-tracked muons and other particles depositing charge in the SDs. The amount of noise, and thereby, also the height of the dip, is affected by a changing liner reflectivity in a different manner than the muons, and thus, the dip-to-hump ratio also is dependent on the reflectivity of *Tyvek*.

The three quantities have undergone the following changes: The dip-to-hump ratio has increased by approximately $15\%$ over $8-9$ years, the muon decay time has decreased by the same amount over nine years, (see figure 2.8), as has the AoP ratio (see figure 2.9). As has been mentioned above, this has significant impact on the energy scales of SDs, meaning that there is a possible drift in the measured energy deposition on the SDs. Therefore, it is vital to quantifiably understand the origins of these changes and how they exactly affect the measured SD signals, so that they can be predicted and corrected for in further analyses. In [10], simulations of the above quantities showed that a $2\%$ decrease of *Tyvek* reflectivity could account the decrease.
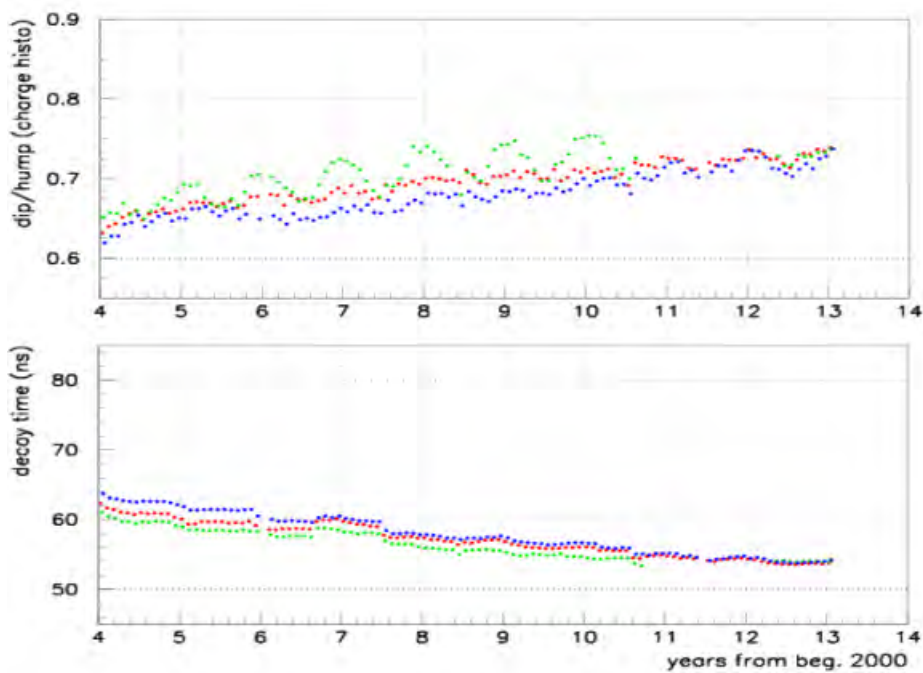


Figure 2.8: The change of the dip-to-hump ratio and the muon decay time over $8-9$ years (From: [10])

There are also several papers, which focus on the long-term change of the SD performance. They will be summarised in the following.

In [11], Billoir simulates the detector response to a signal and computes the effects of a changing reflectivity of the liner wall, namely the *Tyvek*, in order to check how this affects the calibration of the detector. He found that a decrease of the AOP ratio could lead to an overestimation of the signals at increasing altitude and distance of the air shower to the detector, but calls for more direct investigation of the effects of a variable reflectivity on this matter, especially on how this changes the dependence of the zenith angle of the incident air shower particles on the detector response.

H. Wahlberg has examined the long-term changes of the AoP and the effects freezing events of the SDs have on their performance in [12] and [13] (the latter together with R. Sato). In the former paper, he pointed out that the AoP is used as measure for the water qualitiy and *Tyvek* reflectivity. He found that the AoP decreases after the SD is put into operation, but then stabilises, and that the behaviour can be described adequately with an exponential fit with a characteristic time of approximately 1.5 years. He also observed that the decrease is always smaller than $20\%$, which should not negatively affect the operation of the SD. In the later paper, he showed that there is a permanent decrease of the AoP after events, which correlate with the freezing of the water in the SDs (see 2.9), but cannot be explained yet.

9

Steps to delay the formation of ice have been tested and a polyurethane thermal isolation seems to fulfill this task.
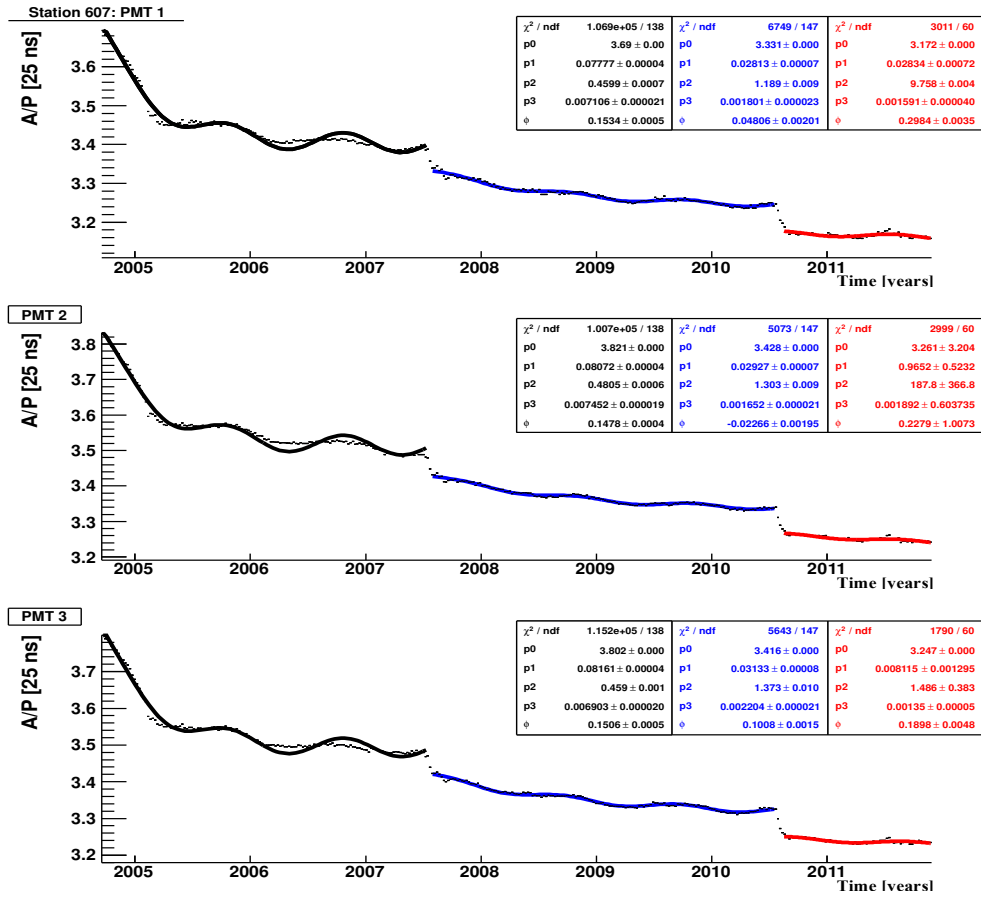


Figure 2.9: Evolution of the AoP ratio over the course of seven years (2005 to 2012); the sharp drops in Argentinian winter in 2007 and 2010 correspond to cold times with freezing observed in detectors (From: [13] )

Now that the influence of a changing reflectivity of *Tyvek* has been shown, its properties have to be discussed. It is not only important to know those related to the PAO, but also some of the general properties of *Tyvek*. In addition, *Tyvek*'s reflective properties, as determined in earlier papers are of interest, in order to know what the status quo of its investigation is. In the next section, therefore, these properties will be presented.

## 2.3 General and reflective properties of *Tyvek*

*Tyvek* is not only used for the PAO, but finds application in a wide variety of fields ranging from air and water resistant covers for construction and cars, over envelopes and other packaging, to protective apparel in medicine and for personnel of high-risk occupations [2].

According to *DuPont*® [2], *Tyvek* consists of "continuous and very fine fibers of 100 percent high-density polyethylene that are randomly distributed and nondirectional", which "are first flash spun, then laid as a web on a moving bed before being bonded together by heat and pressure". They promote it as chemically inert to most acids and salts, deformation-resistant at room temperature, dimensionally stable (sheet dimension change less than $0.01$ % with rising humidity at constant temperature), moisture-resistant and an adequate liquid barrier, while being ultra light and extremely flexible [2]. These features, along with its reflective properties make *Tyvek* very suitable as the coating for the liner of the water tanks at the PAO.

Furthermore, several of *Tyvek*'s reflective properties have been studied in earlier papers, the results of which are relevant for this thesis both as an information source to determine the measurement techniques, and as a reference to test the compatibility of the results obtained in this thesis, and will, thus, be summarised below.

The reflectivity of *Tyvek* has both a specular and a diffuse component. The angular dependence on a measured signal reflected off its surface is usually parametrised by the sum of a Gaussian depicting the specular component and cos-component, which stands for the diffuse component (clarification further below in section 4):

$$I = P_1 \cdot \exp\left[-\frac{(\theta - \theta_i)^2}{2\sigma^2}\right] + P_2 \cdot \cos(\theta) \quad [14],$$ (2.1)

where $P_1$ and $P_2$ give the amplitudes of each component, $\theta$ is the measured reflection angle, $\theta_i$ is the mean angle of the specular reflectance, and should be equal to the incident angle $\theta_i$, and $\sigma$ is the width of the Gaussian and characterises the surface roughness.

In [14] by Filevich et al. the angular dependence of relative intensity of the specular component was analysed by measuring the signal of light reflected off *Tyvek* both in air and immersed in water as a function of the reflection angle for different incident angles. They used a slightly modified version of equation 2.1 (the Gaussian peak was set as free parametre and a phase displacement of half of the incident angle was added to the cos-term) to calculate the change of the specular amplitude relative to the diffuse amplitude. The results were, that this ratio is the lowest for an incidence angle of $\theta_i = 45°$, that it is hardly dependent on the wavelength (measurements were conducted both for visible and UV light), and that the shape of the signal shows hardly any difference for air or for water except for there being no need to introduce a phase shift for the data acquired from the *Tyvek* in air.

In their paper [15], Arteaga Velázquez, Vázquez López and Zepeda also compared the specular and diffuse component of the reflectivity of *Tyvek*, with special focus on the influence of optical anisotropies in the diffuse component with respect to a rotation of the *Tyvek* sample perpendicular to the surface normal and note that there is an anti-correlation between *Tyvek*'s specular and diffuse component, i.e. the larger the one component, the smaller the other.

Ling-Yu et al. applied an alternative way to measure the optical parametres of *Tyvek* in [16]. They use a description of the angular dependence of the reflectivity different from equation 2.1, namely the so-called *UNIFIED* model, which describes the reflection and transmission of light for rough surfaces:

$$I = R(\theta_i, n) \cdot [C_{sl} \cdot g(\alpha_r, 0, \sigma_\alpha) + C_{ss} \cdot \delta(\theta_i - \theta_r) \cdot \delta(\phi_r) + C_{bs} \cdot \delta(\theta_i + \theta_r) \cdot \delta(\phi_r) + C_{dl} \cdot \cos(\theta_r)] \quad [16],$$ (2.2)

where $R(\theta_i, n)$ is the total reflectivity of the surface, which is a function of the incidence angle $\theta_i$ and the refractive index of the medium $n$, in which the surface is situated. $C_{sl}$ is the so-called specular lobe constant, depicting a diffused specular component of the surface around the angle $\alpha_r$ (analogous to the specular component in equation 2.1), i.e. the angle between the average and the microfacet surface normals $\vec{n}$ and $\vec{n'}$, which exist due to the surface's roughness.

Therefore, $\alpha_r$ characterises this very roughness. $C_{ss}$ is the so-called specular spike constant, which gives the part of the light exactly spectrally reflected off the average surface, and $C_{ss}$, the backscatter spike constant, represents the part of the light exactly scattered back from the average surface. $C_{dl}$ stands for the diffuse lobe constant and thereby for the diffusely reflecting component of the surface. The constants are constrained by

$$C_{sl} + C_{ss} + C_{bs} + C_{dl} = 1 \quad [16].\tag{2.3}$$

The quantities $\theta_r$ and $\phi_r$ are the reflection angle and the angle between the projection on the average surface and the plane of incidence, respectively. The latter angle is introduced, because specular reflection or backscattering only takes place if said angle is zero. The other parametres are rather straight-forward when regarding figure 2.10, which depicts all components in a polar plot (left) and definitions of the geometrical parametres (angles and surface normals) in the coordinate system used; thus, they need not be further discussed.
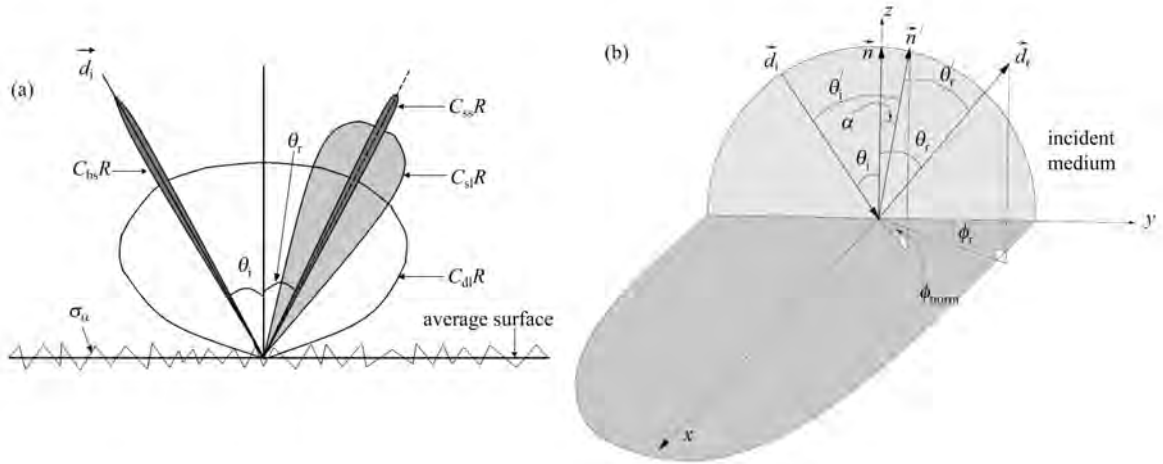


Figure 2.10: a) Polar plot qualitatively illustrating the components in the UNIFIED model; b) The coordinate system used and definition of geometrical parameters (From: [16])

The team reflected a pulsed laser with repetition frequency of 2.5 GHz and a pulse width of 70 ns FWHM off a *Tyvek* surface, filling an entire 2.8 m × 1.2 m × 1.3 m water tank, in which the detector (a PMT) was placed at the bottom in such a way, that light underwent both single and multiple reflections before reaching it. They measured the signal over a time interval of 500 ns and 5 Gigasamples/s and fitted the UNIFIED model onto the signal using MC simulations with a value for the total reflectivity of $R = 98$ %, which they obtained from previous measurements. They put special focus on the values for $C_{sl}$ and $\sigma_\alpha$ as the signal shape seems to depend mostly on them, and found the best agreement for $C_{sl} = 85$ % and $\sigma_\alpha = 0.06$, indicating that the diffused specular component by far constitutes the largest fraction of the total reflectivity of *Tyvek* − the remaining components only make up 15% (see equation 2.3).

Similar conclusions were drawn by Alvaro Chavarria in his thesis [17], where he conducted the same kinds of measurements as in the papers preceding the former. His main finding was that the combination of a specular and a diffuse component of the reflectivity of *Tyvek*, as portrayed in equation 2.1, corresponds well with the measured signals in air and under water if the angle of incidence is smaller than 40°; at higher angles the tail of the data is missed. But in addition, he points out that the diffuse part had often been over-estimated in earlier MC simulations pre-dating that thesis, and that the diffused specular component plays a larger role than had been estimated, and even dominates in water.

Measuring the different components is of special interest. While the setup for the other components is rather straight-forward, the theoretical background of the integrating sphere, which was used for measuring the diffuse reflectivity of *Tyvek*, will have to be elucidated. This will be done in the following section.

## 2.4  The integrating sphere

For this section I will use [18] as reference, in which the theory of the integrating sphere and its applications is described in great detail.

The integrating sphere is an instrument mainly used to measure optical radiation. It has many applications, inter alia as a measurement device for the diffuse reflectivity $\rho$ of surfaces. Its theory yields a simple way of calculating $\rho$, and the experimental setup is relatively easy to implement.

First, we start off with a diffusely reflecting surface. A surface like this follows *Lambert's cosine law* (named after *Johann Heinrich Lambert* (1728 – 1777) ), which states that the radiant intensity of light reflected off such a surface is proportional to the cosine of the angle of reflection $\theta_r$ (angle between the propagation direction and the surface normal):

$$I \propto \cos(\theta_r) \quad \rightarrow \quad I(\theta_r) = I_0 \cdot \cos(\theta_r), \tag{2.4}$$

where $I_0$ is the intensity of the light prior the reflection hitting the surface perpendicularly.

Consider two differential elements of such surfaces $dA_1$ and $dA_2$ which are seperated by a distance $S$ (see figure 2.11 a) ). The (differential) exchange factor $dF_{dA_1-dA_2}$ is the measure of the fraction of the energy leaving $dA_1$ and arriving at $dA_2$ and is given by

$$dF_{dA_1-dA_2} = \frac{\cos(\theta_1) \cdot \cos(\theta_2)}{\pi S^2} dA_2, \tag{2.5}$$

where $\theta_1$ and $\theta_2$ are the angles between the connecting vector of the two surfaces $\vec{S}$ and the surface normals of $dA_1$ and $dA_2$, respectively. This equation follows directly from *Lambert's cosine law*, when considering that the radiant intensity of the light reflected off $dA_1$ is proportional to $\cos(\theta_1)$ and the radiant intensity of that light hitting $dA_2$ is proportional to $\cos(\theta_2)$; this product is then simply normalised through division by the area of a circle with the radius $S$.
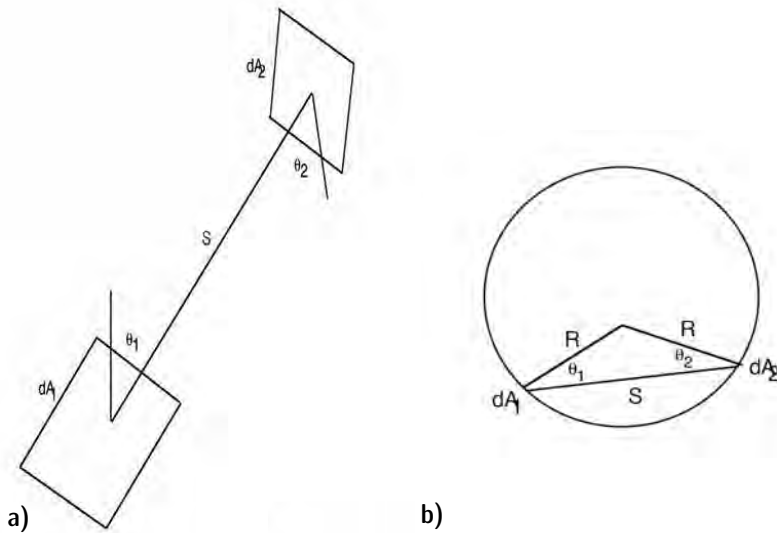


Figure 2.11: a) Illustration of two differential surfaces $dA_1$ and $dA_2$ separated by a distance $S$; b) Illustration of the differential surfaces inside a sphere with radius $R$ (From: [18])

If $dA_1$ and $dA_2$ are differential elements inside a sphere (see figure 2.11 b) ), one can express $S$ as follows:

$$S = 2R \cdot \cos(\theta_1) = 2R \cdot \cos(\theta_2), \tag{2.6}$$

where $R$ is the radius of the sphere. Thus, $\mathrm{d}F_{\mathrm{d}A_1 - \mathrm{d}A_2}$ can be expressed in the following way:

$$\mathrm{d}F_{\mathrm{d}A_1 - \mathrm{d}A_2} = \frac{\mathrm{d}A_2}{4\pi \cdot R^2}. \tag{2.7}$$

Expanding $\mathrm{d}A_2$ to a finite area $A_2$ through integration over said area yields

$$F_{A_1 - A_2} = \frac{A_2}{4\pi \cdot R^2} = \frac{A_2}{A_{\mathrm{S}}}, \tag{2.8}$$

where $A_{\mathrm{S}}$ is the surface area of the sphere's inside. Note that the above expression is independent of $\mathrm{d}A_1$, the exchange factor is, thus, independent of the direction of the incoming light, it is simply given by the fraction the area $A_2$ covers of the whole inside surface area $A_{\mathrm{S}}$.

Next, the radiance $L$ of the sphere needs to be calculated, starting off with the general expression

$$L = \frac{\Phi_{\mathrm{i}} \cdot \rho}{2\pi \cdot A_0}, \tag{2.9}$$

where $\Phi_{\mathrm{i}}$ is the incoming flux, $\rho$ is the (diffuse) reflectivity of the surface, $\pi$ expresses the total projected solid angle (half a unit sphere) and $A_0$ is the illuminated area. At the $n$th reflection the incoming flux $\Phi_{\mathrm{n}}$ is given by

$$\Phi_{\mathrm{n}} = \Phi_{\mathrm{n}-1} \cdot \rho \cdot \frac{A_0}{A_{\mathrm{S}}}. \tag{2.10}$$

Suppose that the sphere is consumed by two ports, an input port $A_{\mathrm{i}}$ and an exit port $A_{\mathrm{e}}$. $A_0$ is then given by $A_{\mathrm{s}} - (A_{\mathrm{i}} + A_{\mathrm{e}})$. With

$$f = \frac{A_{\mathrm{i}} + A_{\mathrm{e}}}{A_{\mathrm{S}}} \tag{2.11}$$

as the port fraction equation 2.10 can be expressed as follows:

$$\Phi_{\mathrm{n}} = \Phi_{\mathrm{n}-1} \cdot \rho \cdot (1 - f). \tag{2.12}$$

Iterating $n$ times yields

$$\Phi_{\mathrm{n}} = \Phi_{\mathrm{i}} \cdot \rho^{n-1} \cdot (1 - f)^{n-1} \tag{2.13}$$

After $n$ reflections, the total flux therefore is

$$\Phi_{\mathrm{tot.}} = \sum_{k=0}^{n} \Phi_{\mathrm{k}+1} = \Phi_{\mathrm{i}} \cdot \sum_{k=0}^{n} (\rho \cdot (1 - f))^n \tag{2.14}$$

With $n \to \infty$ we get a geometric series which converges to:

$$\Phi_{\text{tot.},\infty} = \Phi_{\text{i}} \cdot \frac{\rho \cdot (1 - f)}{1 - \rho \cdot (1 - f)}. \tag{2.15}$$

For the radiance of the sphere surface $L_{\text{S}}$ follows

$$L = \frac{\Phi_{\text{i}}}{2\pi \cdot A_{\text{S}} \cdot (1 - f)} \cdot \frac{\rho \cdot (1 - f)}{1 - \rho \cdot (1 - f)} = \frac{\Phi_{\text{i}}}{2\pi \cdot A_{\text{S}}} \cdot \frac{\rho}{1 - \rho \cdot (1 - f)} = \frac{\Phi_{\text{i}}}{2\pi \cdot A_{\text{S}}} \cdot M, \tag{2.16}$$

where

$$M = \frac{\rho}{1 - \rho \cdot (1 - f)} \tag{2.17}$$

is the so-called surface multiplier.

Now let us consider the case that there are $m$ ports with reflectvities $\rho_{\text{k}} \neq 0$, $k = 1, 2, 3, ..., m$. Each port opening consumes the port fraction $f_{\text{k}} = \dfrac{A_{\text{k}}}{A_{\text{S}}}$. The reflectivity of the sphere wall is $\rho_{\text{S}} \neq 0$. Equation 2.17 then needs to be modified thusly:

$$M = \frac{\rho_0}{1 - \rho_{\text{S}} \cdot (1 - \sum_{k=0}^{m} f_{\text{k}}) - \sum_{k=0}^{m} \rho_{\text{k}} \cdot f_{\text{k}}} = \frac{\rho_0}{1 - \bar{\rho}}, \tag{2.18}$$

where $\rho_0$ is the reflectivity of the wall hit by the incident flux $\Phi_{\text{i}}$, and

$$\bar{\rho} = \rho_{\text{S}} \cdot \left(1 - \sum_{k=0}^{m} f_{\text{k}}\right) + \sum_{k=0}^{m} \rho_{\text{k}} \cdot f_{\text{k}} \tag{2.19}$$

is the average reflectivity of the total sphere.

In the experimental setup which was used in the measurements conducted for this thesis were three ports: the aforementioned input and exit ports $A_{\text{i}}$ and $A_{\text{e}}$, both with negligible reflectivities, and a sample port $A_{\text{s}}$, in which the sample probe — whose reflectivity $\rho_{\text{s}}$ is to be measured — is placed. The average reflectivity can then be expressed as follows:

$$\bar{\rho} = \rho_{\text{S}} \cdot (1 - (f_{\text{i}} + f_{\text{e}} + f_{\text{s}})) + \rho_{\text{s}} \cdot f_{\text{s}}. \tag{2.20}$$

The basic conduct is as follows: The radiance (or rather intensity $I$ in Amperes) is measured once with the sample port filled with a reference material of known reflectivity $\rho_{\text{r}}$, and once filled with the sample of unknown reflectivity $\rho_{\text{s}}$ (e.g. *Tyvek*), $L_{\text{r}}$ and $L_{\text{s}}$.

Two types of setup are of insterest. In the former, the reference and the sample are measured through the same port, and thus, need to be substituted (the setup is called the *substitution sphere*; see figure 2.12 a) ). One can further differentiate between two cases. Depending on the material of the surface area, which is hit by the incident flux $\Phi_{\text{i}}$, the calculation of the reflectivity is somewhat different. For both cases the radiance is measured for both the reference and the sample material, and the ratio between the two is calculated:

$$\frac{L_{\text{s}}}{L_{\text{r}}} = \frac{\frac{\Phi_{\text{i}}}{2\pi \cdot A_{\text{S}}} \cdot M_{\text{s}}}{\frac{\Phi_{\text{i}}}{2\pi \cdot A_{\text{S}}} \cdot M_{\text{r}}} = \frac{\frac{\rho_0}{1 - \bar{\rho}_{\text{s}}}}{\frac{\rho_0}{1 - \bar{\rho}_{\text{r}}}}. \tag{2.21}$$

If the initial reflection takes place on the the sample port area ($\rho_0 = \rho_s$ or $\rho_0 = \rho_r$), the ratio becomes:

$$\frac{L_s}{L_r} = \frac{\rho_s}{\rho_r} \cdot \frac{1 - \bar{\rho}_r}{1 - \bar{\rho}_s}.$$

(2.22)

If the first reflection takes place on surface material of the sphere, the ratio changes to

$$\frac{L_s}{L_r} = \frac{1 - \bar{\rho}_r}{1 - \bar{\rho}_s}.$$

(2.23)

This equation shows that the substitution sphere should not include the first reflection occurring on the sample or reference surface, respectively. Variation between $\rho_s$ and $\rho_r$ has little measurable impact, and thus, the measurements are burdened by large uncertainties. Generally, while the substitution sphere is relatively easy to actualise, the determination of $\rho_s$ bears the significant problem of being dependent on the reflectivity of the sphere surface material $\rho_S$, which also must be exactly known. Even if known, the average reflectivity is generally very hard to determine. In most cases it must approximated, possibly yielding gratuitous systematic uncertainties.

A sightly more complicated setup, in which the sample port is separated into two parts consuming different parts of the sphere, called the *comparison sphere*, can be used as an alternative (see figure 2.12). The reference material is placed in front of one port and the sample material in front of the other. Then the light source is directed such a way that the first reflection is on the reference material or the sample material, respectively. For each arrangement the radiance is measured and the ratio is calculated. Since the overall setup of the sphere's surface hasn't changed between the two measurments, the averge reflectance is the same for the both. The ratio is thus given by

$$\frac{L_s}{L_r} = \frac{\rho_s}{\rho_r}.$$

(2.24)

This equation is extremely simple and the only quantity which needs to be known is the reflectivity of the reference material $\rho_r$. It is above all independent of the material, with which the sphere is coated. This is actually just an idealisation, which is only the case if the radiance can be measured with any desired accuracy. This not being the case, there is in fact a dependence on the sphere surface material.
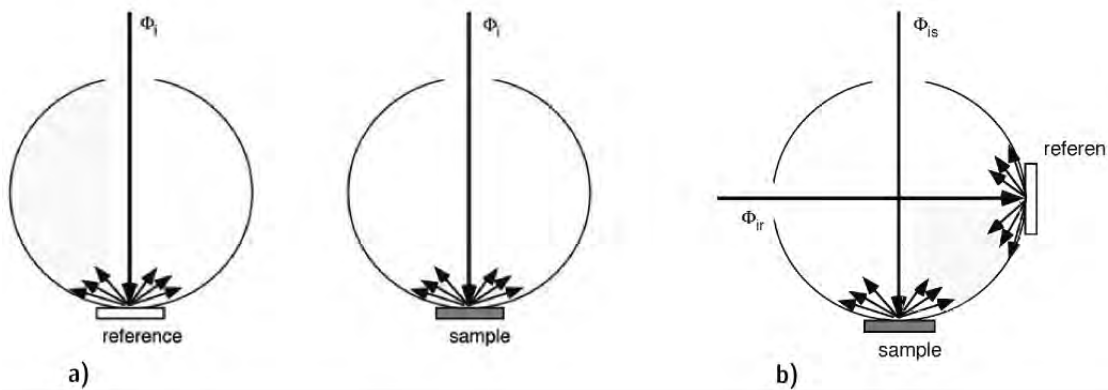


Figure 2.12: a) Illustration of the substitution sphere; b) Illustration of the comparison sphere

For one part, the surface multiplier $M = \frac{\rho_0}{1 - \bar{\rho}}$ is a function of $\rho_S$. Furthermore, $M$ is also a function of the total port fraction $\sum_k f_k$, and the port fraction and reflectivity of the sample.

Graph 2.13 shows $M$ as a function of the sphere reflectivity $\rho_S$ for different values of the sample reflectivity $\rho_s$. The sample constitutes 4 % of the total surface area, the total port fraction is at 5 %. The setup was assumed to be that of the

substitution sphere, which means that $\rho_0 = \rho_S$. One can see that for $\rho_S < 90\ \%$ $M$ is smaller than 10; for a relatively weak incoming flux (as will be the case for my measurements) the total surface radiance $L_S$ will be quite small. It is, therefore, desirable to have a surface reflectivity of at least $\rho_S = 90\ \%$.
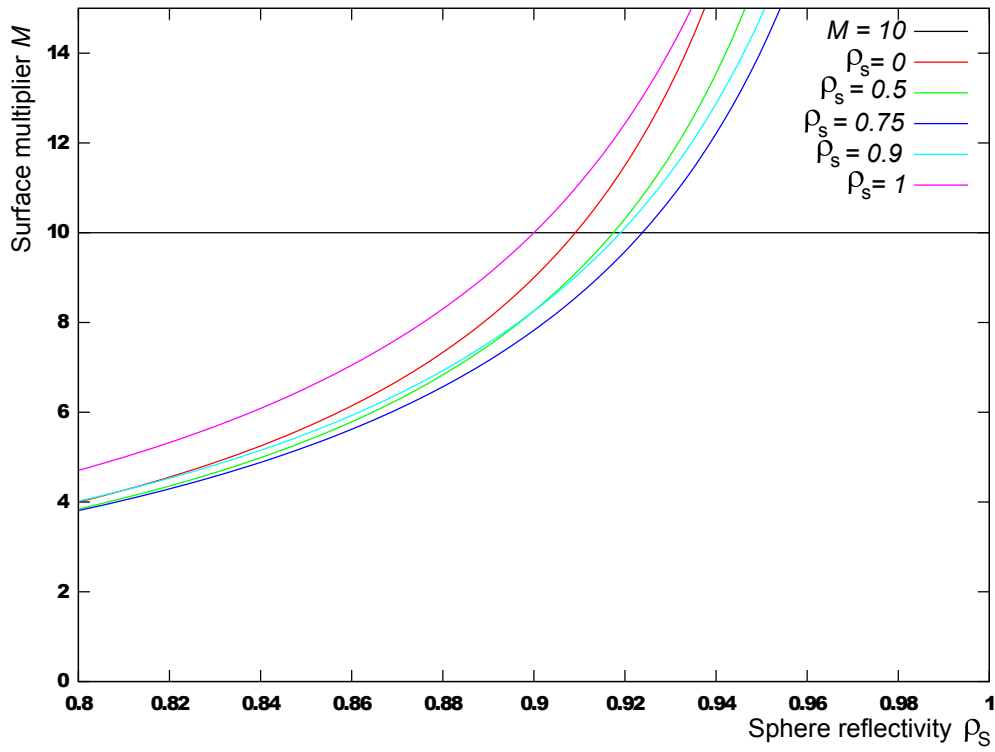


Figure 2.13: Surface multiplier $M$ as a function of the surface reflectivity $\rho_S$ for different values of the sample reflectivity $\rho_s$

In graph 2.14, $M$ as a function of the total port fraction $f$ is plotted with $\rho_S < 90\ \%$. Since $M$ is smallest when all ports have zero reflectivity, $\rho_s$ is chosen accordingly. Here one can see a value of $M < 8$ for port fractions larger than $5\ \%$. Therefore, in order for the amplification to be approximately an order of magnitude or more, $f$ should not exceed $5\ \%$.

Another factor which needs to be considered is the sphere size. The surface radiance $L_S$ is inversely proportional to the surface area $A_S$ (see equation 2.16), or to the square of the radius or diameter $R_S^2$ or $D_S^2$, respectively. Thus, the size of the sphere needs to be as small as possible.

It is also of interest to know how well one can apply equation 2.24 to the substitution sphere (more exactly, to the setup, in which the initial reflection does not take place on the sample or reference surface, respectively). Figure 2.15 shows the relative deviation of equations 2.22 and 2.24, and illustrates the systematic error. If the difference between $\rho_s$ and $\rho_r$ is smaller than $5\ \%$, then the systematic error does not exceed 2%. If the $\rho_s < \rho_r$, then applying said equation always underestimates the result.
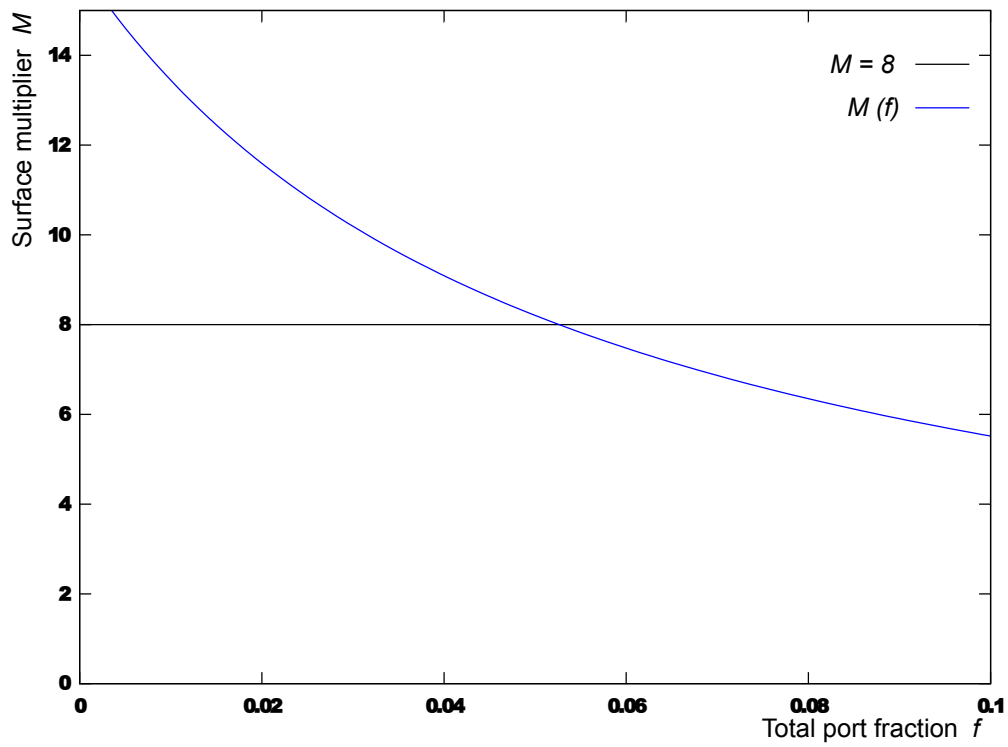
Figure 2.14: Surface multiplier $M$ as a function of the total port fraction $f$
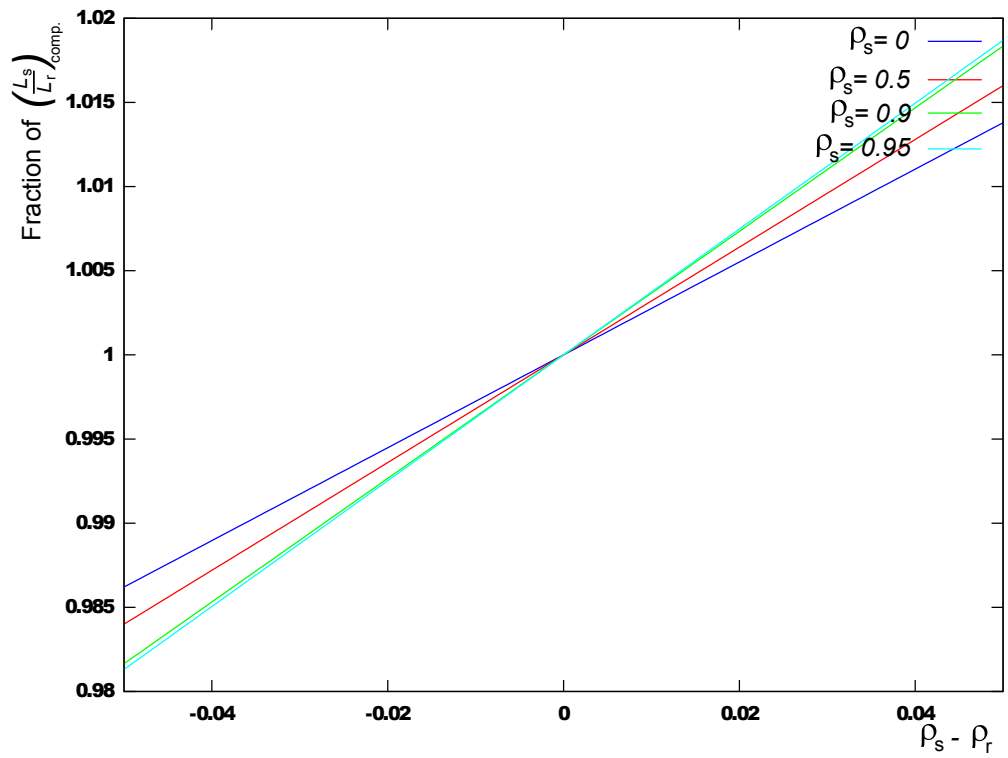


Figure 2.15: Relative deviation of equations 2.22 and 2.24

# Chapter 3

# Investigating microscopic structural differences among used and unused samples of *Tyvek* with SEM images

In the introduction, I mentioned that observations of the macroscopic structure of the *Tyvek*, which was used in the SDs at the PAO, were made, namely black "spots" and kinks or wrinkles were visible in the fabric (see figures 3.1 and A.1). This made the surface more inhomogeneous, which might lead to a lower reflectivity that varies strongly in small scales. These assumptions are confirmed in chapter 5 section 2.1.



Figure 3.1: a) Sample of unused Tyvek; b) Sample of used *Tyvek*; structural differences are visible, especially the black "spots" in the used sample

In this chapter, the origins of the structural changes on microscopic scales is investigated. Scanning electron microscope (SEM) scans of a used and an unused *Tyvek* sample (see figure 3.1) have been done to search for clear structural changes in the fibres themselves.

For this, small samples of the two types of *Tyvek* depicted in figure 3.1 were cut out. Regions were picked, which were characteristic of the macroscopic differences observed between the two: A black "spot" was cut out from the used sample, while it mattered less, which part was cut out of the unused sample, because it is sufficiently homogeneous on macroscopic scales.

The scans were performed with the help of *Jan Gasse* from the department of condensed matter physics can be seen in figures 3.2 and 3.3.
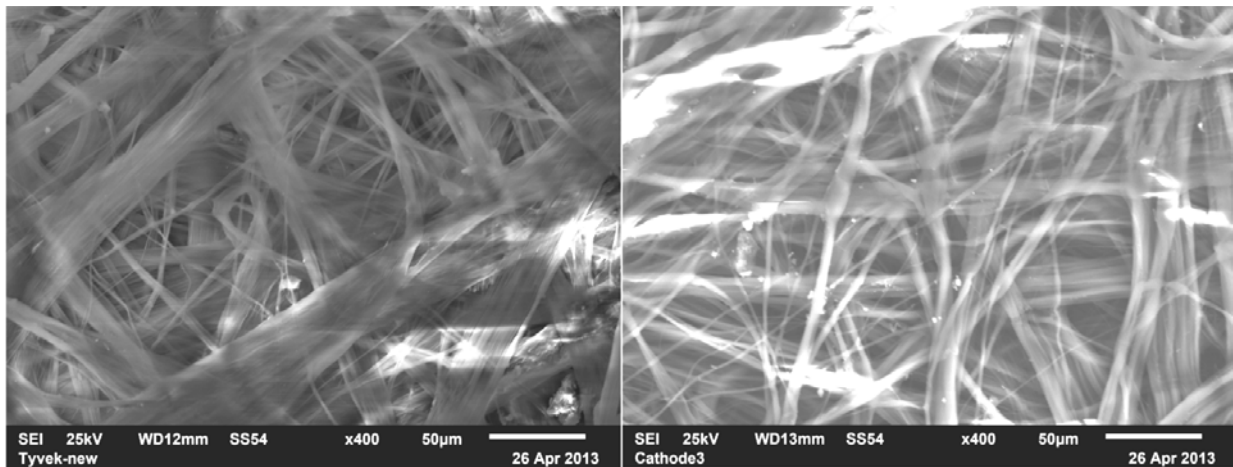


Figure 3.2: SEM scan of unused (left) and used (right) *Tyvek* with 400-fold zoom
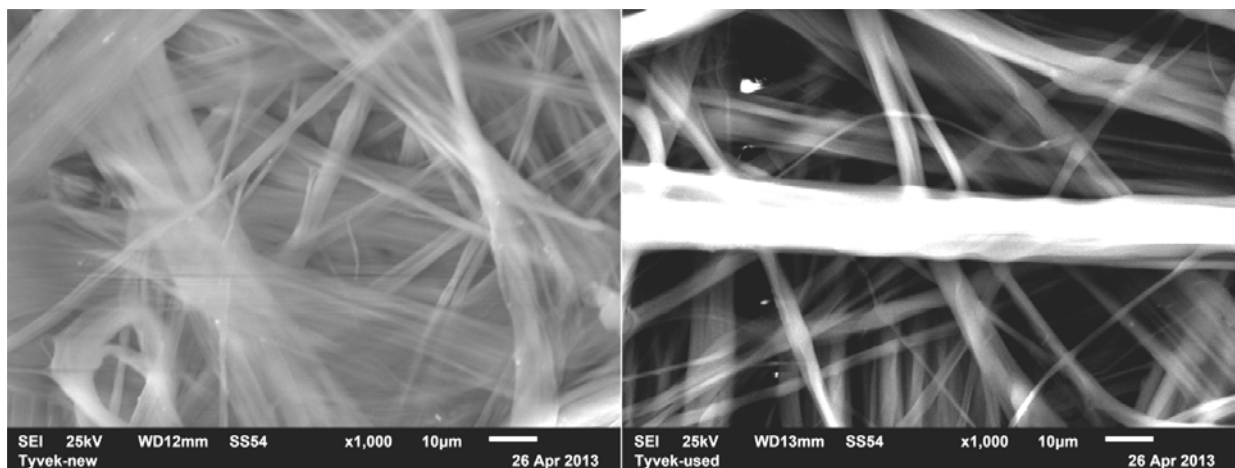


Figure 3.3: SEM scan of unused (left) and used (right) *Tyvek* with 1000-fold zoom

First, it needs to be noted that the light spots in the figures came about due to local charging of the fibres through the electrons, leading to a deflection of further electrons from that region.

In both scans no obvious differences in the fibres' structure is visible. No torn fibres or contamination by foreign particles greater than for the unused sample can be detected for the used sample. The only difference is a smaller density of fibres for the used sample.

We can thus infer that, being exposed to water under pressure and under varying temperature does not tear or damage the fibres of *Tyvek*, but rather causes them to stretch and shift, leading to a lower density of fibres, locally. On larger scales, the fibre density distribution is less homogeneous, eventually leading to the black "spots" observed for the used *Tyvek* samples. However, no explanation for the origins of the wrinkles can be given.

# Chapter 4

# Diffuse reflectivity measurements with the integrating sphere

For measuring the diffuse reflectivity of *Tyvek*, the integrating sphere is a suitable device, given the conditions discussed in chapter 2 section 4: The diffuse reflectivity of the sphere wall $\rho_S$ has to be larger than 90 %, the total port fraction $f$ must not exceed 5 %, the size of the sphere must be as small as possible.

Due to the fact that *Tyvek* is very inhomogeneous and has a strongly varying reflectivity over small length scales (up to 20 %), the *Tyvek* sample area has to be sufficiently large, in order for the measured reflectivity over that area to correspond to the actual average reflectivity. In chapter 5 section 1.2, the appropriate area is determined to be approximately 7 cm $\times$ 7 cm.

## 4.1   Measurements with a large Styrofoam coated sphere

If one wishes to measure the reflectivity of the entire sample surface within one measurement, there is a lower limit to the sphere size. Since this area must not occupy more than 5 % of the total sphere surface area, the minimum inner radius of the sphere is $R_S = \sqrt{\frac{49 \text{ cm}^2}{5 \text{ %} \cdot 4\pi}} \approx 9$ cm.

Since experiments both in air and under water are to be performed, the material used for the sphere wall coating has to be insoluble in water. This already posed a problem, because the material, which was used in prior reflectivity measurements, was $BaSu_4$, a soluble material. It can be used, however, for a "test sphere" to determine a suitable material, as its reflective properties are known (see figure A.5 in the appendix). Unfortunately, non-soluble paints with sufficiently high reflectivity turn out to be financially unviable, which, in effect, only allows for the investigation of a single material, namely that used for building/constructing the actual sphere, Styrofoam$^{\text{TM}}$.

For measuring Styrofoam's wavelength-dependent reflectivity $\rho(\lambda)$ the following setup was used: A light source (a deuterium-tungsten combination, see figure A.2) coupled to a monochromator is induced through an input port into a $BaSu_4$-coated styrofoam sphere with radius $R = 17$ cm. Slightly less than a right angle from the input port along the cross sectional area, going through the centre of the input port and the opposite wall, the exit port with an area of 5.8 mm $\times$ 5.8 mm occupied by a photo diode of equal size coupled with an amperemetre for detecting the photo current (see figures A.3 and A.4), and the sample port are located on opposite sides (see figure 4.1).

This setup is that of the *substitution sphere* (see chapter 2 section 4), for which equation 2.22 holds for the calculation of the reflectivity. The angle is kept smaller than 90° to prevent incident light from entering the detector, because the approximation of an infinite amount of reflections ($n \rightarrow \infty$) only applies for large values of $n$. Deuterium and tungsten lamps are used in a combination in order for the light intensity, and thereby for the measured photo current
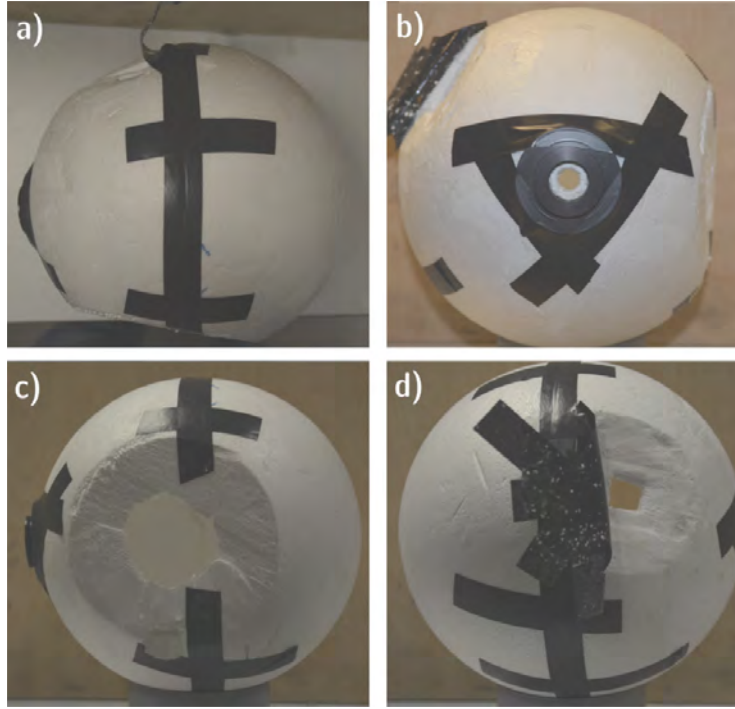
Figure 4.1: a) Top view of the integrating sphere; b) Front view of the input port; c) Side view of the sample port; d) Side view of the exit port

to be sufficiently high for wavelengths ranging from 180 nm to 800 nm. While deuterium's spectrum spans the lower wavelengths, tungsten becomes dominant for higher wavelengths. However, the light sources have different intensities with that of the tungsten source having a higher maximum intensity, but also being variable. For the intensities of the two light sources to be comparable, the intensity of the latter must be reduced to about 15 % of its maximum intensity. The current measured both for Styrofoam and a reference sample, which for reasons of convenience was $BaSu_4$, were then compared. Figure 4.2 shows the complete setup as photographs and as a schematic.

The photo current as a function of the wavelength of light for both Styrofoam and $BaSu_4$ is plotted in 4.3, and the ratio of the two in figure 4.4.

The ratio of Styrofoam and $BaSu_4$ is consistently smaller than 1 with a minimum at about 36 % for 240 nm. Of special interest is the UV to blue wavelength range, because this is the range of highest intensity of the Cherenkov light and the range of highest efficiency of the PMTs in the SDs at the PAO. The ratio does not reach 90 % up to wavelengths above $\approx 550$nm. From this we can conclude that Styrofoam's reflectivity is lower than 90 % in the interesting wavelength range, given the following approximation:

$$\left( \frac{L_\mathrm{s}}{L_\mathrm{r}} \right)_\mathrm{subs.} \leq \left( \frac{L_\mathrm{s}}{L_\mathrm{r}} \right)_\mathrm{comp.} , \tag{4.1}$$

where $\left( \frac{L_\mathrm{s}}{L_\mathrm{r}} \right)_\mathrm{comp.}$ and $\left( \frac{L_\mathrm{s}}{L_\mathrm{r}} \right)_\mathrm{subs.}$ are the radiance ratios from equations 2.22 and 2.24, respectively, in chapter 2 section 4. This is a justified assumption, as can be seen in figure 2.15 from the same section; the reflectivity of Styrofoam is always smaller than that of $BaSu_4$. Therefore, the operability of the integrating sphere is not given for the inner walls consisting of Styrofoam.
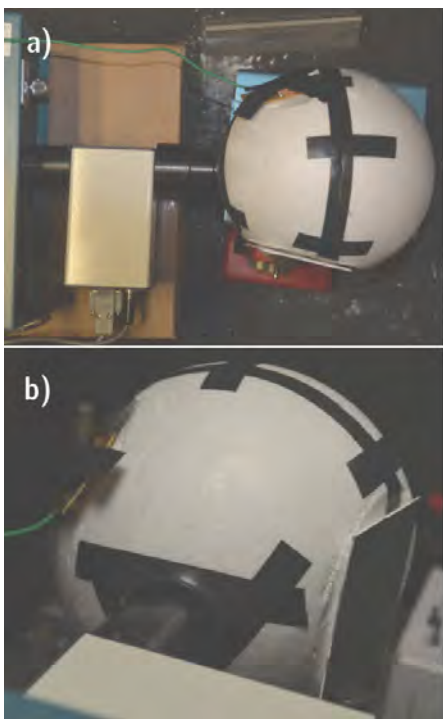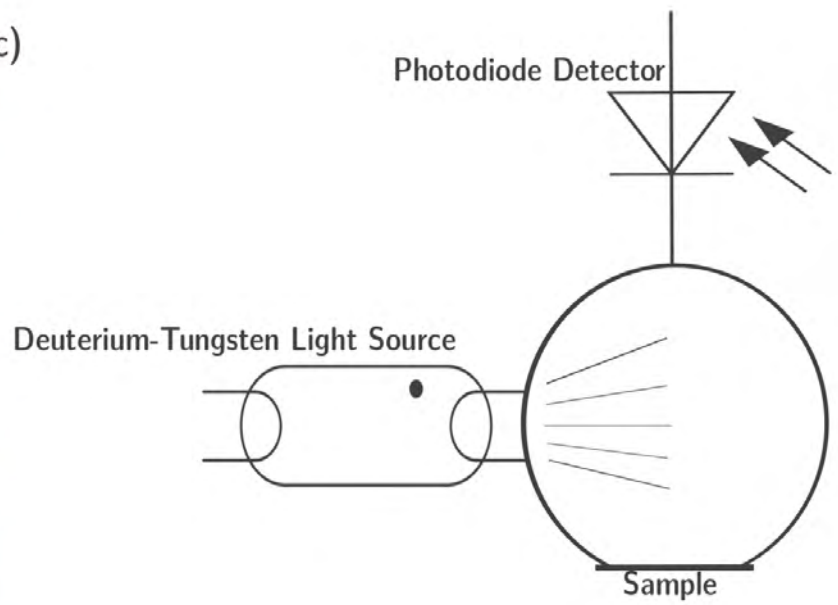
Figure 4.2: a) Top view of the integrating sphere setup; b) Front view of the integrating sphere setup; c) Schematic of setup
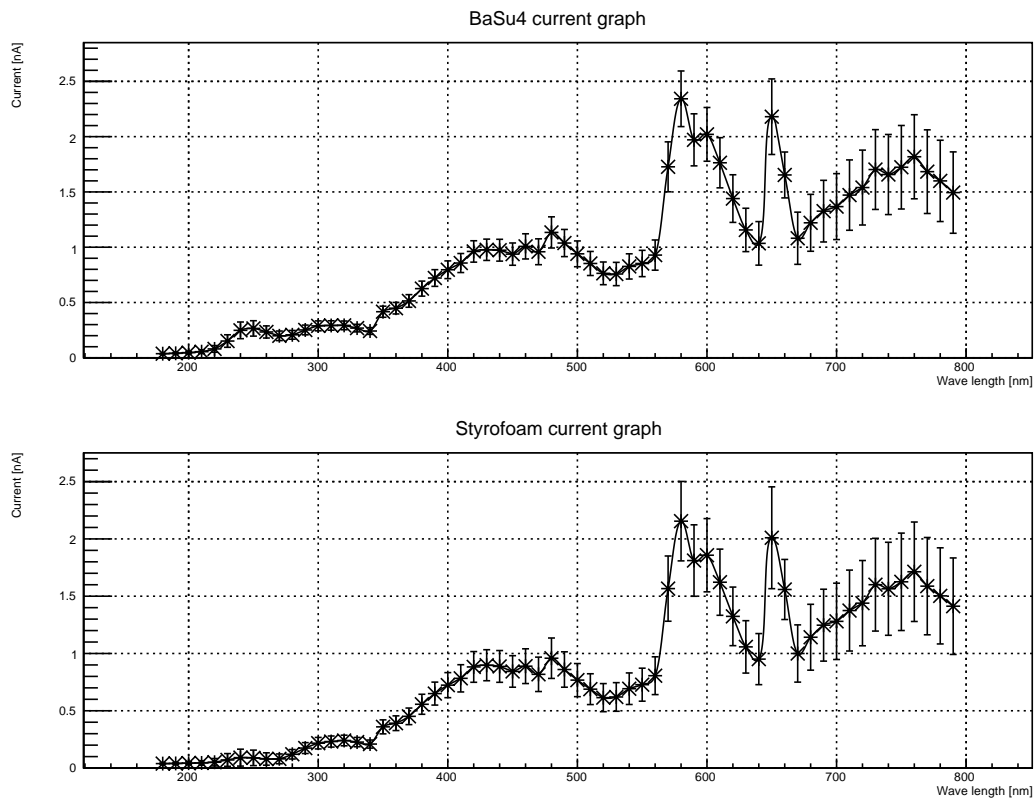
Figure 4.3: a) Measured photo current as a function of wavelength for the BaSu$_4$ sample; b) Measured photo current as a function of wavelength for the Styrofoam sample
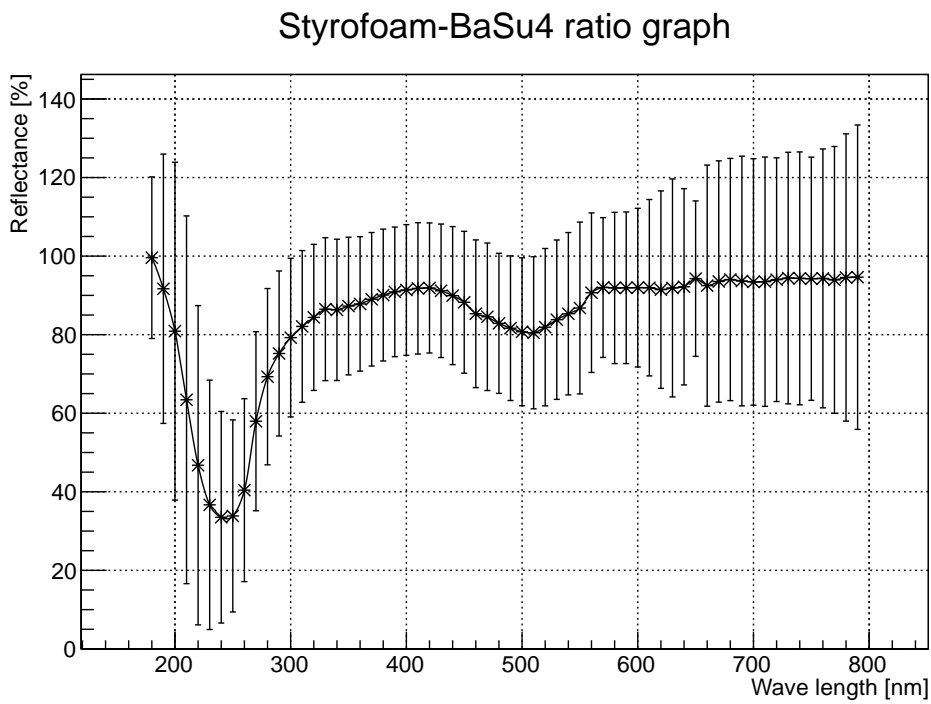


Figure 4.4: Ratio of the Styrofoam and BaSu$_4$ spectra

## 4.2 Measurements with a small sphere coated with *Tyvek*

The large sphere had to be abandoned because no suitable material was found with which it could be coated, given time and budget constraints. An alternative is to build a small sphere (radius $R = 3.32 \pm 0.05$ cm; see figure 4.5), which admittedly decreases the maximum port sizes, especially of the sample port. Yet, by scanning the whole surface in small step sizes (the determination of adequate step sizes and sample areas will be discussed in chapter 5 section 1), a larger surface could be measured. Furthermore, in order to maximise the sample port size, the input and exit port were limited to the size of optical fibres (about 1 mm in diameter), through which light was inserted into the sphere and collected for measurement. This allowed for the sample port to have a diameter of 1 cm.



Figure 4.5: a) Photograph of the input port of the small sphere with an optical fibre stuck into it; b) Photograph of the sample port of the small sphere; c) Photograph of the exit port of the small sphere with an optical fibre stuck into it; d) Photograph of the small sphere divided in two halves; all ports are in the left hemisphere, with the central point depicting the input port, the large whole depicting the sample port and the point at the left depicting the exit port

A suitable sphere wall material was *Tyvek*, but not the type employed in SD tanks. Prerequisite measurements had shown that this kind of *Tyvek* has a reflectivity around 90%. While it would have been difficult to cover large surface areas homogeneously due to the fact, that *Tyvek* had to be clothed instead of painted on to the walls, the measurement procedure, especially when measuring in water, was simplified by a small sphere.

The setup is in principle the same as for the large sphere (see figure 4.2), the only difference being that a different light source was used, namely a 405 nm pulsed laser diode from *ALPHALAS GmbH*, set at a repetition rate of 10 MHz in order to get a "quasi-continuous" signal (see figure A.6). The same photo diode connected to the same amperemetre used in the previous section, was used as a detector. The advantage of using a laser is that its angle of radiation allows for a large fraction of light to be coupled into the fibre, while at the same time having a high intensity, allowing for a high signal. This had to be done due to the fact that the photo current, when measuring in water, decreases by more than an order of magnitude, which would lead to the signal being in the range of the dark current of the amperemetre. While a schematic of the setup is not necessary, figure 4.6 shows photographs of it. The *Tyvek* samples were cut out in suitable

sizes, to ensure that they could be stuck onto the sphere and fully covering the sample port (see figure A.7). The goal was to obtain comparative results of used and unused *Tyvek* rather than absolute values. After all, the properties of unused *Tyvek* have been studied already. The measurement was conducted both in air and in water. For the measurements, 15 regions of each sample type were measured, thus the final photo current is the average of 15 single measurements.
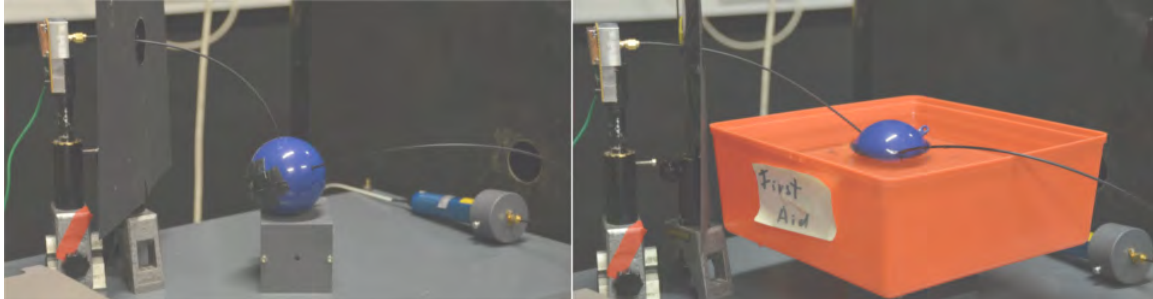


Figure 4.6: a) Photograph of the setup with the small integrating sphere for measurements of *Tyvek* in air; b) Photograph of the setup with the small integrating sphere for measurements of *Tyvek* in water; the *Tyvek* was stuck with black Sellotape onto the sample port, the right fibre is connected to the laser, and the the left fibre to the photo diode

**Analysis of data**

The average photo current for used *Tyvek*, unused *Tyvek*, and the ratio of the two, both in air and in water is listed in table 4.1. The measurement uncertainty was determined by calculating the standard deviation $\sigma$ from the average current.

Table 4.1: Photo current for used *Tyvek*, unused *Tyvek*, and the ratio of the two, measured with the small integrating sphere, both in air and in water

| Measurement medium | Unused *Tyvek* | Used *Tyvek* | Ratio |
|---|---|---|---|
| Air | $381.2 \cdot (1 \pm 1.48\,\%)$ pA | $376.2 \cdot (1 \pm 1.81\,\%)$ pA | $98.7 \cdot (1 \pm 2.3\,\%)$ % |
| Water | $14.86 \cdot (1 \pm 11.86\,\%)$ pA | $14.38 \cdot (1 \pm 8.45\,\%)$ pA | $96.80 \cdot (1 \pm 8.4\,\%)$ % |

The data shows that used *Tyvek* has a lower diffuse reflectivity than unused *Tyvek*. In air, it is $(1.3 \pm 2.3)$ % lower, in water even less, with $(3.2 \pm 8.4)$ %. Also of interest is the measurement uncertainty. In air, it is about 2.3 % that of the measured ratio; while larger than the average difference itself, it is relatively small, compared to the measurement in water, which has an uncertainty of 8.4 %. Both measurements have a rather large uncertainty, which is mainly due to the inhomogeneity of *Tyvek*. The even larger uncertainty in water has two reasons: Firstly, the samples seem to become more inhomogeneous in water, as black spots become more frequent in recently immersed samples. Secondly, the current fluctuates stronger in water. The former fact produces an uncertainty of about 5 %, the latter, one of about 6.5 %. Underwater measurements limits its significance, so that it is not clear if the difference in reflectivity between used and unused *Tyvek* is larger in water. In addition, one needs to consider further uncertainties due to the fact that equation 2.24 was applied for calculating the relative reflectivity of used *Tyvek*; the obtained result is thereby overestimated (see figure 2.15). The reflectivity is in fact even lower, though not more than 2 % of the calculated value. The measurement uncertainties could have been reduced with more measurements, as $\sigma \propto \frac{1}{\sqrt{n}}$. However, time constraints and the need to scan a sufficiently large surface limit the viability of ever increasing numbers of measurements, as the measurement time is proportional to $n$.

In conclusion, the measurements indicate that used *Tyvek* has a lower diffuse reflectivity in air than unused *Tyvek* of up to about 3 %. While the measurement uncertainty is actually larger than the difference, the data does quantify this difference, though limited in significance. In water the difference might be larger, but so is the measurement uncertainty, so that it cannot be conclusively inferred from the data. While more measurements would have decreased the uncertainties, constraints to the actual feasible number of measurements is set be the measurement time. More significant results would have been obtained with a larger sphere, as larger sample ports can be used.

# Chapter 5

# Specular reflectivity measurements with the reflection probe

Although the diffuse component of *Tyvek*'s reflectivity is of main interest with respect to the PAO, the ageing effects should similarly affect the specular component. A simple setup is given by the so-called *reflection probe*, which is a device consisting of seven optical fibres, of which six are circularly arranged around the seventh central fibre (see schmetic figure 5.3). The six fibres transport injected light to the head of the probe, which irradiates on a given sample surface at a distance of about a millimetre. The surface, in turn, reflects the light back through the centre fibre to a detector. The detector is connected to a PC, which collects and displays the data with the help of a *labview* program. It collects the current of 20 single measurements and calculates the mean and standard deviation, which, in turn, constitute the measurement value and its uncertainty.
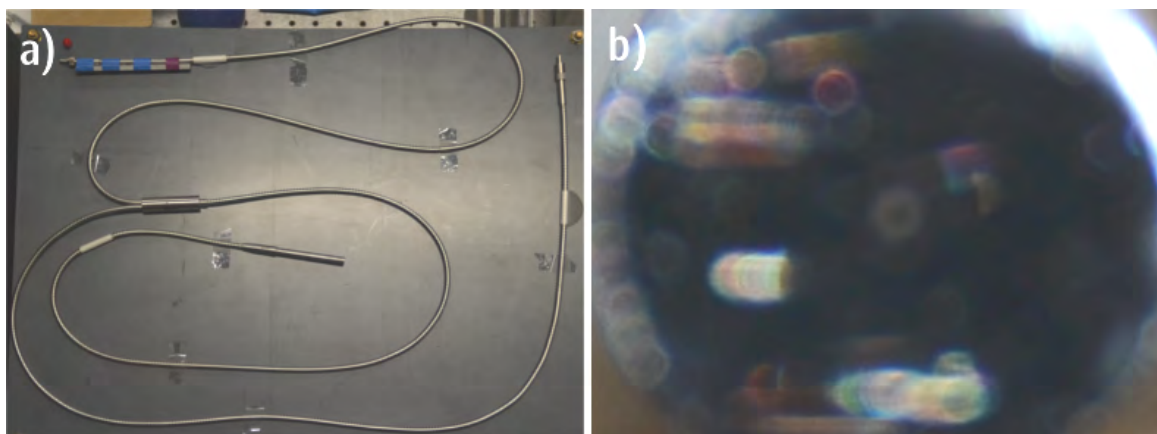


Figure 5.1: a) Photograph of the reflection probe; the light is coupled into the probe (top left) are led to the probe head (centre), reflected from a surface into the probe and led to the "detector end" (top right); b) Photograph of the probe head from the top, the blurred grey ring in the centre is the fibres

For the measurements, the same photo diode used with the integrating sphere (chapter 4), served as the detector. As light source an LED (type $G04 - 187$) with a wavelength of $400$ nm was used and powered with $4$ V (see figure A.8); originally the same deuterium-tungsten light source of the integrating sphere measurements was intended for use but had to be abandoned due to the measured photo current being so weak that it was in the range of the fluctuating dark current, which proved too difficult to correct for. The reflecting surfaces were a mirror and a miro aluminium plate by *alanod* serving as calibration samples, and different samples of *Tyvek*, one set used (i.e. samples extracted from the tank liners of the SDs at the PAO) and the other unused (i.e. fresh samples of the same types of *Tyvek* contained in

the SDs). Figure 5.3 shows both a schematic and photograph of the basic experimental setup (from [19]). Keeping the probe head at a distance from the samples was achieved with a metallic cylinder, in which the probe head was placed (see figure A.9). At the same time it allowed the probe head to radiate perpendicularly on the surface. The cylinder is equipped with a rubber ring at the bottom, which has a high friction coefficient and, thus, keeps its position fixed during measurements (see figure A.9).
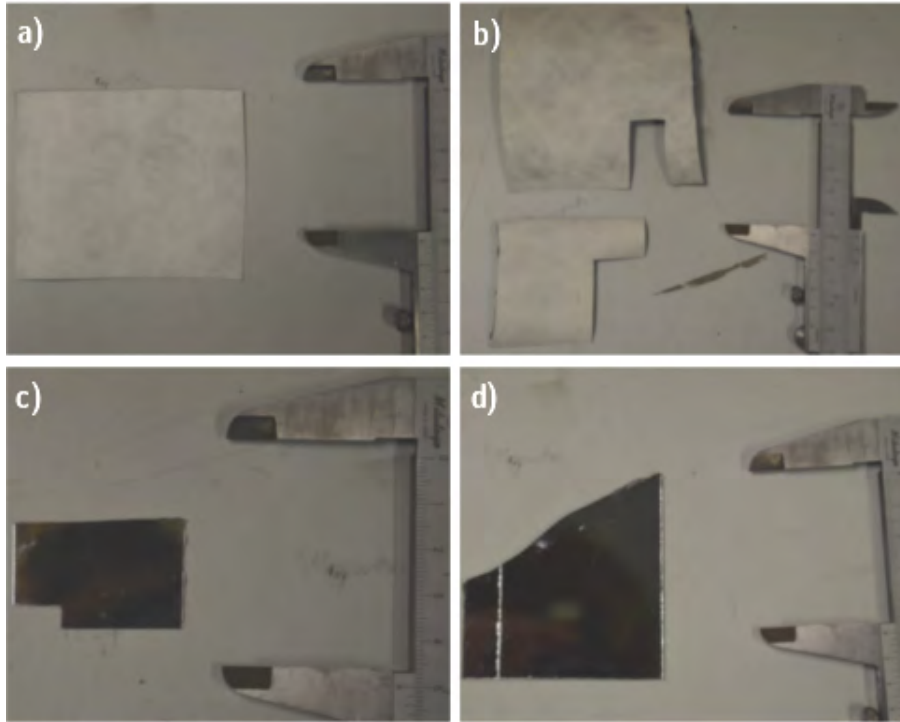


Figure 5.2: a) The *Tyvek* sample(s) used for freezing; b) The used (top) and unused (bottom) *Tyvek* samples; c) The calibration plate; d) The calibration mirror; the calliper was kept at the same setting to allow for a good comparison between the size of the samples

The following main aspects were studied with the presented setup:

- The change of the reflectivity of both used and unused *Tyvek* when immersed in water (directly and after an extended period of time);

- the effects of freezing unused *Tyvek* (both in water and in air);

- the possibility of imitating the vanishing nano bubbles with an ultrasonic bath;

- the difference between used and unused samples of *Tyvek* concerning the dependence of their reflectivity on the distance to the probe head.

Each of these will be described in detail in separate sections. But before we turn to them, some prerequisite measurements, which were performed to minimise the uncertainty of the aforementioned setup, will be presented. Their results will directly be discussed, as they serve the purpose of optimising the setup of the main experiments.

## 5.1 Prerequisite Measurements

Due to the random distribution of the fibres in *Tyvek*, its reflective properties are not homogeneously distributed across the surface, but are subject to local changes. This causes fluctuations in the range of 20 % in the measured
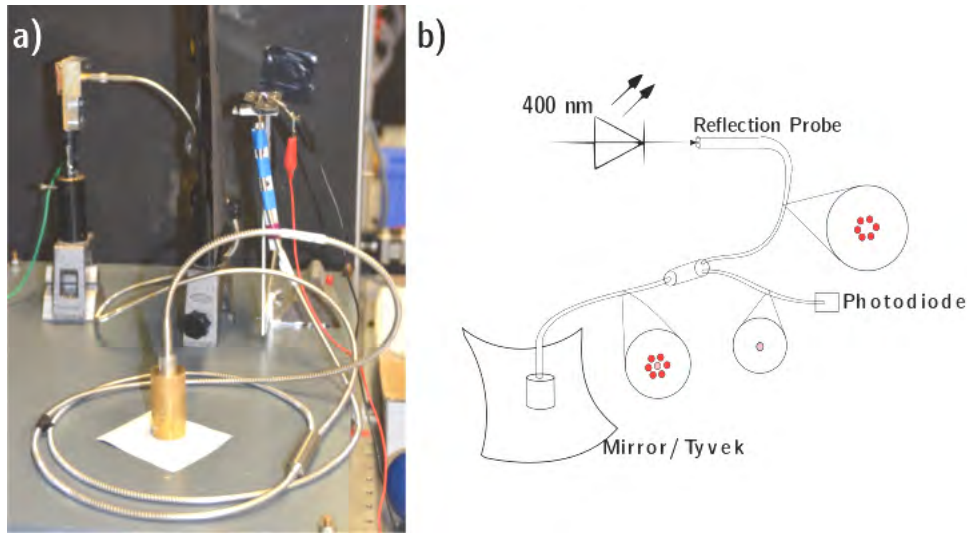
Figure 5.3: a) Photograph of experimental setup; b) Schematic of experimental setup (From: [19]

photo current at different parts of the surface. As a result, there is large measurement uncertainty, which cannot be eliminated. It is important to minimise the influence of other potential sources of error. Two of these sources are the temporal stability of both the radiant intensity of LED and the data acquisition of the photo diode on the one hand, and the size of a measured *Tyvek* sample on the other.

### 5.1.1 LED and photo diode stability

The measured photo current is dependent on the performance of the LED and the photo diode. Both the intensity of the light and the acquisition of data have to be stable over time, because a varying signal will increase the measurement uncertainty of the photo current. While averaging over 20 consecutive measurements corrects for short-term fluctuations, long-term variations need to be examined. To measure the behaviour of the signal over longer periods of time and to determine to what extent this behaviour depends on the LED and the photo diode, respectively, three measurements were conducted, all having their basic implementation in common. In all three cases, the photo current was measured at certain time intervals, ranging from one minute in the beginning to 10 minutes in the end. They merely differ in the way amperemetre and LED, respectively, had been turned on before measurement. In the first one, both devices were turned on simultaneously and directly measured. In the second case, the amperemetre had been on for an extended amount of time and the change of the LED signal was measured. In the third, it was vice versa.

The measured currents at each point of time are plotted in figures 5.4 to 5.6.

A "saturation curve" was fitted onto the data points,

$$I(t) = a \cdot \left(1 - e^{-b \cdot (t-c)}\right), \tag{5.1}$$

where $a$, $b$ and $c$ are fit parametres. The values for each parametre, the $\chi^2/\text{NDF}$ are also displayed in the plot.

The assumption was that the current converges towards a "saturation current" after switching on the LED and the amperemetre. Comparing the three plots, one can see that the fitting curves agree well with the data points for the first two plots in which the influence of the LED is strongest, which confirms the above stated assumption for the two. The "saturation constant", $b$, is also more than one order of magnitude larger for the two than for the third, in which the influence of a varying data acquisition rate of the amperemetre should be visible. This indicates that the behaviour of the signal is caused primarily by the LED. Yet, the agreement is limited, as indicated by the fact that the fitted value of
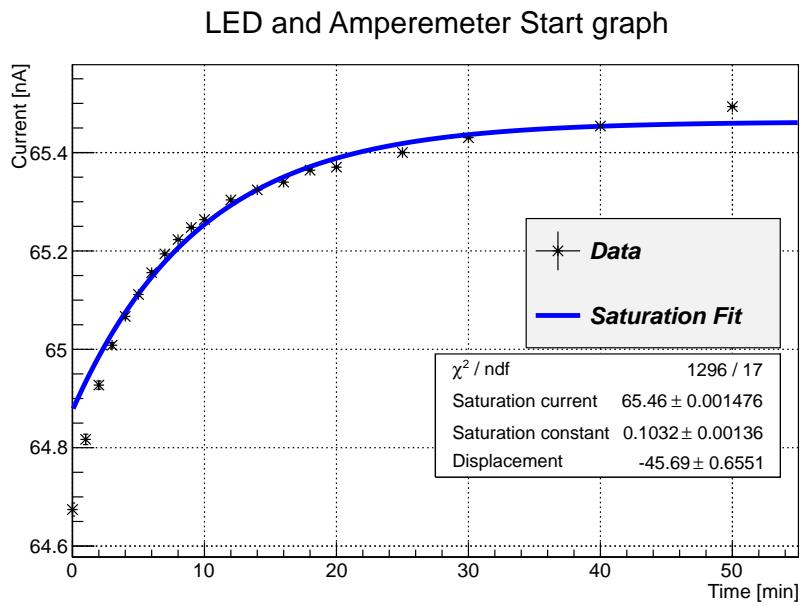
Figure 5.4: The photo current as a function of time after turning on the LED and the amperemetre
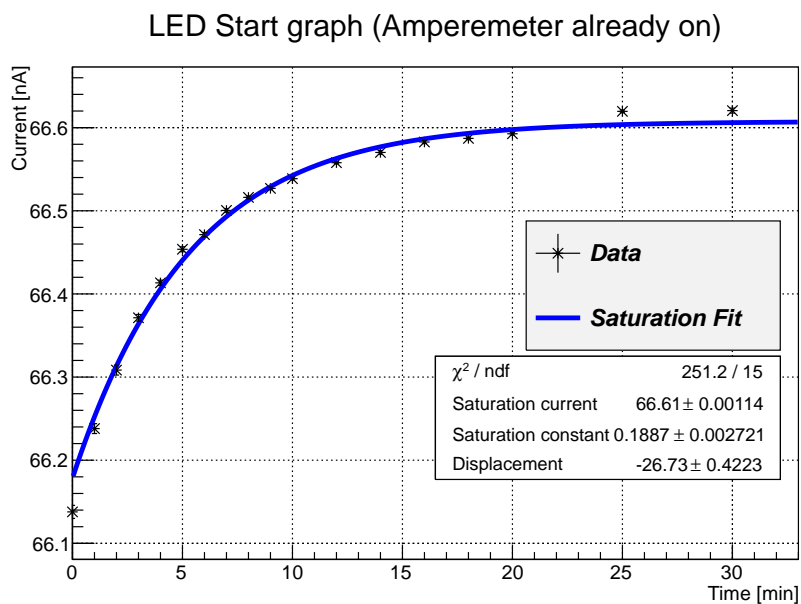


Figure 5.5: The photo current as a function of time after turning on the LED; the amperemetre had been on for several hours beforehand
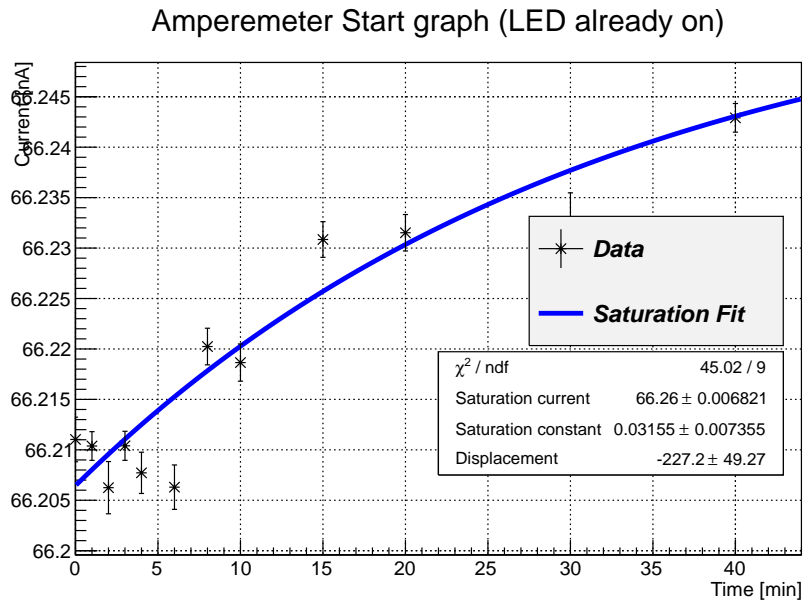
Figure 5.6: The photo current as a function of time after turning on the amperemetre; the LED had been on for several hours beforehand

the "saturation current", $a$, is too low (it is smaller than the later data points), that the values for $b$ vary quite strongly between the first two plots, and that the "time displacement", quantified by the parametre $c$, is unrealistically high; the time measurement was not started immediately after turning on LED and amperemetre, but the power supply was not on for more than 10 minutes before we did start measuring (and certainly not more than 100). In addition, the relatively high values for $\chi^2$/NDF ($1296/17$, $1296/17$ and $45.02/9$, respectively) suggest that the measurement uncertainties have been underestimated; the uncertainty due to the extended time, over which one measurement was performed (about 20 s), was not taken into consideration. Still, the fits are sufficient for these purposes, because it was only necessary to ensure that the signal eventually varies by less than 1 % when measuring over an extended period of time, which certainly is the case. If a measurement series is short (not longer than 10 minutes), then waiting half an hour after switching on the power supply to the LED and the amperemetre guarantees this. For longer measurements (more than an hour) it is recommendable to additionally have the LED switched on for several hours before measuring, in fact, for reasons of practicability, not to switch it off at all between separate measurement series.

### 5.1.2 Size of *Tyvek* sample

When measuring the reflective properties of *Tyvek*, two aspects need to be considered, which result from the fact that the surface of *Tyvek* is very inhomogeneous. On the one hand, a sufficiently large sample needs to be used for the measurements, in order for the resulting data to be representative of the actual reflectivity of *Tyvek*. One the other hand, the sample size cannot be too large; due to the close proximity of the probe head to the reflecting surface, i.e. the *Tyvek*, of $\approx 1$ mm, only a very small fraction of the total surface area can be covered by the reflection probe in a single measurement (an area of $\approx 0.5$ mm$^2$ is lighted by one fibre), which makes it necessary to scan the surface in very small steps (around a centimetre step size). The optimal size needs to be investigated. For this purpose, two samples of almost equal size were cut out of the same sheet of *Tyvek*, then the average photo current over the entire surface of each sample, $I_1$ and $I_2$, was measured. If their deviation is small, around 5 % is sufficient, considering the inhomogeneity of *Tyvek*'s surface, the sample size is representative of the entire sheet. First, a sample size of approximately 7 cm $\times$ 7 cm was cut out and measured. The ratio of the measured photo currents for each sample was calculated. The value of this ratio is

$$\frac{I_1}{I_2} = 1.03 \pm 0.09.$$

The deviance from 1 is sufficiently small; the used sample size is adequate for measuring the properties of *Tyvek*. The resulting number of single measurements, which need to be performed are in the order of 20, which is acceptable.In conclusion, the procedure for the reflectivity measurements is defined: Measuring the reflectivity of a sample means measuring the current over the whole sample area, i.e. performing the approximately 20 single measurements, and subsequently normalising to the current measured for a certain calibration probe (the mirror or the plate; the exact one will be stated in the given measurement series).

## 5.2 Reflectivity of both used and unused *Tyvek* when immersed in water

The first experiment is investigating the effects that the immersion of both used and unused *Tyvek* in water has on its reflectivity. Three different states will be compared: the reflectivity of *Tyvek* in air, in water directly after it has been immersed, and after an extended period of time (after 1 and 2 weeks, respectively). The point of measuring the reflectivity of *Tyvek* underwater after an extended time period, was to test the nano-bubble hypothesis. Therefore, the samples were not removed from the water after a measurement series was finished. To measure the reflectivity in air, the probe head was placed on a sample of used and unused *Tyvek*, respectively. In principle, the same was done for the underwater measurements, just with the *Tyvek* samples and the probe head being immersed in water. The water needed to be as pure as possible, which is why deionised water was used. To account for the inhomogeneity, while at the same time keeping the measurement time at a feasible length, the measurement procedure, as defined in section 1.2 was applied, measuring at approximately 20 positions, scanning the entire sample surface.

**Analysis of Data**

The photo currents for used and unused *Tyvek* in air and under water measured both directly after immersion and 5 and 9 days afterwards, were normalised to the measured current of the calibration mirror in air and under water, respectively, to calculate their relative reflectivity (with regards to the calibration mirror). They are listed in table A.1. Figure 5.7 gives a qualitative illustration of the development of the reflectivity of *Tyvek* over the 9 days. An exponential decay curve:

$$I(t) = a \cdot e^{-b \cdot t} + c, \tag{5.2}$$

where $a, b, c$ are fit parametres, was fitted onto the data points from the underwater measurements both of the used and unused sample.
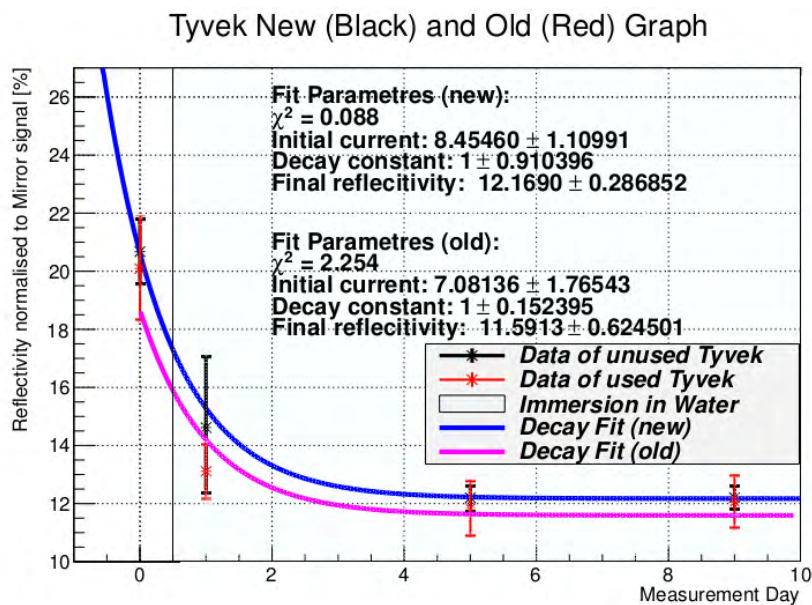


Figure 5.7: Illustration of the change of the reflectivity of used and unused samples of *Tyvek* in air and in water (both samples directly after immersion and after 5 and 9 days, respectively)

In air, the used sample shows a lower reflectivity of 97 % with respect to the unused sample with a standard deviation approximately 1.5 times higher. First of all, a lower reflectivity of the used *Tyvek* sample was expected, as it was thought

to have decreased over the years while installed in the SD. Yet, it needs to be said, that because of the inhomogeneity of the samples, the difference between the samples is still within their margins of error. The higher standard deviation also conforms well with our expectations as it is a measure of the inhomogeneity of the surface, which was observed to be higher for the used sample (see chapter 3).

When immersing the samples in water, the reflectivity decreases to about two thirds for the used sample and to 70 % for the unused sample of the value in air, showing that *Tyvek* has a worse specular reflectivity under water than in air. The reflectivity of the used sample was only about 90 % that of the unused sample. Notable is the fact that the standard deviation of the unused sample tripled, while it halved for the used one, making that of the former higher than that of the latter. An explanation for this result cannot be given. A measuring error is, however, unlikely, as a repeated measurement confirmed the result.

After 5 days, the reflectivity of both samples further decreased by about 10 % of the values measured directly after immersion, or by about 2 % absolutely. The standard deviation of the unused sample fell to even lower values than in air, while it remained the same with about 5 % for the used sample. These values remained approximately the same after 9 days.

These observations agree well with the measured behaviour of the AoP in the SD tanks: A decrease of reflectivity of *Tyvek* in water over time of about 10 % can be measured and it seems to converge towards a final value, namely $12.17 \pm 0.29$ % for unused, and $11.59 \pm 0.62$ % for used *Tyvek*. However, the characterstic time, signified by the decay constant, is significantly lower than the 1.5 years found obtained from the SD tank data. The decrease measured in the detectors does not only appear to be caused by dissipating nano bubbles, but also by a decreasing *Tyvek* reflectivity, which is a lot slower and is the contributing factor to the determined characteristic time. Therefore, our data is compatible with the nano bubble hypothesis.

## 5.3   Variation of the distance of the probe head to the sample

In the fourth experiment, the effects of varying the distance of the probe head to the sample has on the measured photo current were studied. The amount of stray light that can be collected by the centre fibre is expected to vary with the distance, because the angle, with which light can be reflected in the central fibre, decreases with the distance. The amount of stray light reflected, in turn, depends on the proportions the diffuse and the specular each constitute of the total reflectivity of the sample. Thus, differences in the behaviour, that the current shows with changing distance, could give some qualitative insight into that proportion. The measurements were conducted for used and unused samples of *Tyvek*, which both had been immersed in water and treated in an ultrasonic bath with the goal of eliminating nano bubbles from the surface.

The variation of the distance is achieved with the help of additional "capsules", namely small cylinders, of varying height (step size of 0.1 mm), which could be placed on the larger cylinder (see figure A.10). It needs to be mentioned that the height of the large cylinder alone is not sufficient to keep the probe head from touching the sample surface, so that one of the capsules was needed for all the preceding measurements, as well. There were 9 of them available, which were marked with numbers 1 to 11 (numbers 8 and 9 were skipped), indicating the resulting additional distance to approximately 1 mm in units of 0.1 mm that the probe head would have to the surface. The "default" capsule, which was used for the preceding measurements was that labelled with 3 (making the distance of the probe head to the sample $\approx 1.3$ mm). For each capsule the photo current was measured both for a used and an unused sample. The measurements were performed twice for each sample, as changing the capsules, for which the probe head had to be removed from the cylinder, was suspected to lead to a slight shift of the part of the sample illuminated by the probe head. Simply leaving the cylinder stationary and re-entering the probe head in the cylinder after changing the capsules was problematic insofar as the the rubber rings, that allowed the cylinder to stay fixed on the surface, caused a relatively closed volume inside the ring. This would have caused a reduced pressure when trying to remove the head as the volume was being increased, and overpressure when trying to re-insert the head as the volume was being compressed. Both acts caused the emergence of observable tiny bubbles, so that the re-occurrence of nano bubbles on the surface could not be excluded. Lifting the cylinder in order to avoid this problem, in turn, would definitely lead to a shift of its position, meaning that a different part of the sample surface would be reflecting the emitted light from the probe head. Since *Tyvek* is very inhomogeneous, even in small scales, this would shed doubt on the expressiveness of the resulting data. Therefore,

both "imperfect" measurements were conducted, in one of them, the cylinder was left stationary and in the other lifted slightly, hazarding the consequences of the emerging bubbles for one, and the shifting sample position for the other.

**Analysis of data**

The results of the measurements are plotted in figure 5.8 for unused *Tyvek* and in figure 5.9 for used *Tyvek*, the top plot depicting the measured current with the lifted cylinder, the bottom one that with stationary cylinder.
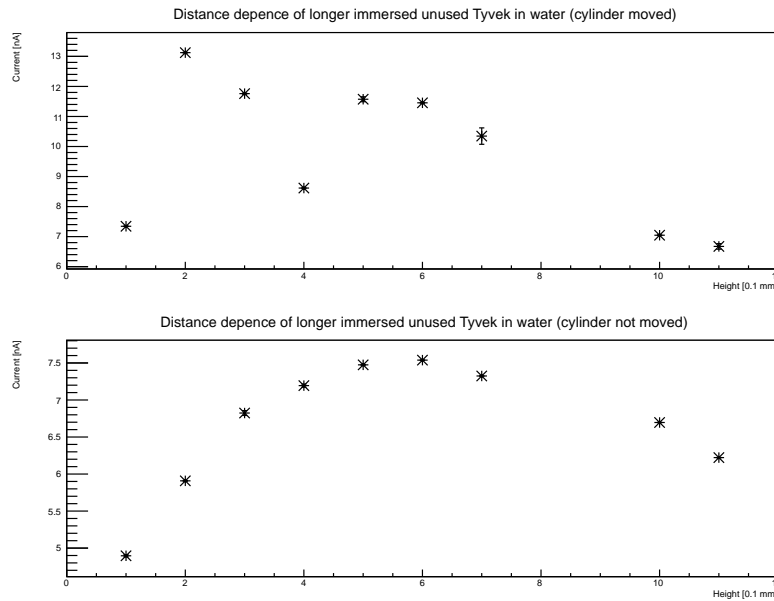


Figure 5.8: The change of the reflectivity of unused *Tyvek* with the distance of the probe head to the sample; the top plot depicts the lifted cylinder measurement, the bottom plot the stationary cylinder measurement

As expected, the top plot shows a fluctuating signal, which can be ascribed to the fact that different parts of the sample with different reflectivities were illuminated by the probe head, which is best visible for the unused *Tyvek* sample. These measurements cannot be considered for giving insight into the qualitative proportions of the diffuse and specular components of *Tyvek*'s total reflectivity. The plots for the stationary cylinder, however, show a more continuous behaviour with a maximum current around pin 5 for the used sample and pin 6 for the unused sample. If one assumes that the existence of nano bubbles does not influence the proportion of the diffuse versus the specular component, the plot indicates that less stray light is emitted for the unused than for used sample, implying a higher specular component for the unused sample. However, if the emerging bubbles, when changing the capsule, do cause nano bubbles, then one would expect the specular component to increase, as stray light, caused mainly by the diffuse component, is further suppressed due to the fact that the bubbles create a thin air film on the surface, which reduces the angular range of transmittance at the transition from air to water. A higher specular component would then imply a higher overall fibre density of unused *Tyvek*, which is in agreement with the results from section 1. In addition, one needs to take into account that, the measurements were performed on a small area of the surface, which is not necessarily representative of the entire surface. Thus the measured dependence on the distance of the probe head, could very well differ, if measured over a larger sample surface. Since the difference in the position of the maximum between used and unused *Tyvek* is merely 0.1 mm, one cannot definitively say that the composition of the diffuse and specular components of the total reflectivity differs between the two.
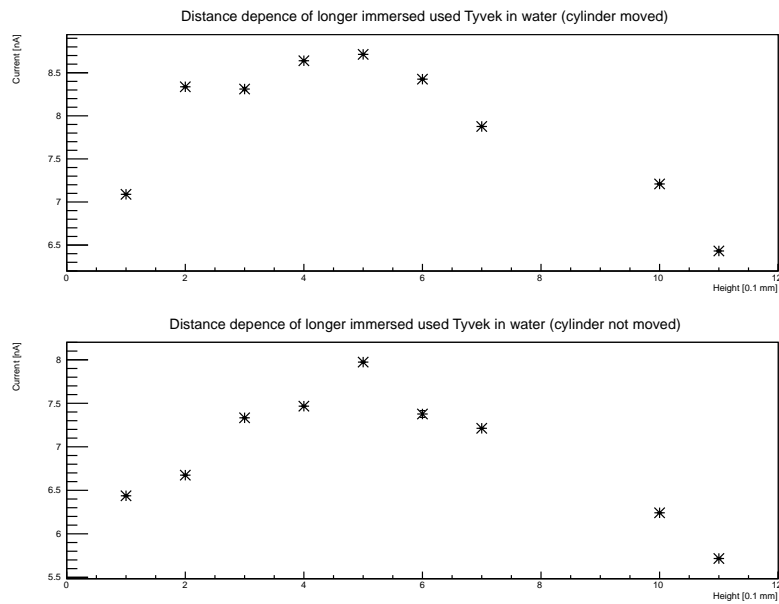
Figure 5.9: The change of the reflectivity of used *Tyvek* with the distance of the probe head to the sample; the top plot depicts the lifted cylinder measurement, the bottom plot the stationary cylinder measurement

## 5.4 Freezing unused *Tyvek*

The second experiment was testing the effects of freezing *Tyvek*. For this purpose, two samples of an unused roll, one immersed in water and one left in air, were placed in a freezer and frozen to down to the same sub-zero (approximately $-18\,°C$) temperature over a few days. After that, the samples were removed, thawed and eventually measured in air with the reflection probe. Figure 5.10 shows a photograph of both samples after removed from the freezer.
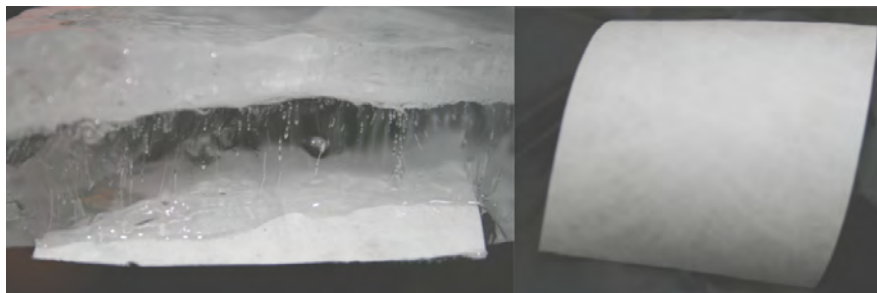


Figure 5.10: a) Photograph of *Tyvek* sample frozen in water b) Photograph of *Tyvek* sample frozen in air

The experiment was performed twice, because in the first measurement series there was a curling up of the sample that was left air, while being cooled down (see figure 5.10 b) ). When trying to bend it back, cracking noises were perceivable, indicating a possible embrittling of the sample, which in turn could have lead to change in the reflectivity of the *Tyvek*, if some of its fibres tore in the process of bending. To test this suspicion, a third sample from the same role was used, which was stuck onto a flat surface, so that it could not bend while cooling down, and compared to the "free" sample in air.

**Analysis of data**

Tables A.2 and A.3 show the relative reflectivity of the three samples with respect to the calibration mirror before and after freezing for both measurement series. As a side remark, it is worth mentioning, that the values measured before freezing in the first series were also used in the prerequisite measurements (section 1) to determine a suitable sample size.

As the data from the measurement before freezing the samples was used for finding the ideal sample size, it comes as no surprise that the reflectivity of all three samples is approximately the same. This does not change significantly after freezing. For the first measurement series, one sees that the reflectivity hardly changes (a relative change of about 3 % and an absolute change of 0.63 % for the sample frozen in air, and a relative change of about 7 % and an absolute change of 1.35 % for that frozen in water), nor does it vary much among the different samples (a relative difference of about 3 % and an absolute difference of 0.62 % before freezing and a relative difference of about 6 % and an absolute difference of 1.36 % after freezing). In the second measurement series, one can observe the same behaviour, when comparing the two different samples cooled down in air (a relative change of about 2 % and an absolute change of 0.48 % for the "free" sample, and a relative change of about 9 % and an absolute change of 1.73 % for the one stuck onto the flat surface while frozen). The underwater sample seems to have a significantly higher reflectivity, even larger than before freezing. As this was not measured in the first series (while the reflectivity is higher than that of the sample in air, the difference is well within the margin of error), and as it contradicts the observed behaviour of the detector performance (the AoP sharply falls after the water in the tank froze), I assume that this is a measurement error rather than a real effect of freezing *Tyvek* in water.

We can therefore say that freezing *Tyvek* in and of itself does not affect the reflective properties to any measurable degree. Neither the expanding water or ice, nor the curving of the sample in air, leads to a detectable, let alone consistent change of its reflectivity. The strongly reduced AoP, which was observed for the SDs, therefore, does not stem from the mere freezing process. I suspect that this is more likely an effect, which comes about for large quantities of water in the confined space of the tank. This could, for example, be an increased pressure on the liner caused by the expanding water or ice, while cooling down, which could not be simulated with our experimental setup. Further measurements need to be conducted for this purpose.

## 5.5 Effects of an ultrasonic bath

Even if the reflectivity of the *Tyvek* changed over time when immersed in water, this would not be sufficient evidence of there having been nano bubbles on the surface, which eventually detached. An alternative way to test the occurrence of nano bubbles is to treat *Tyvek* in an ultrasonic bath, which would artificially remove them if present: The vibration of the water could cause the bubbles to oscillate and eventually, to detach from the *Tyvek* fibres.

To examine the effects of treating *Tyvek* with an ultrasonic bath, its reflectivity is measured in four steps. First, a sample is immersed in water and directly measured, then it undergoes three treatments in an ultrasonic bath, lasting 6 minutes each with the reflectivity being measured between every such treatment.

**Analysis of data**

The measurement results are plotted in figure 5.11.

The exponential decay curve used in section 2 (see equation 5.2) was fitted onto the data points. The curve converges towards a final value, namely $c$, which represents the reflectivity of *Tyvek*, when all the nano bubbles are removed, if the ultrasonic bath in fact dissipates them.

One can see a clear decrease of the reflectivity, as is expected if nano bubbles are in fact vanishing from the surface. However, several aspects indicate that the ultrasonic bath at the very least does more than just dissipating the nano bubbles, possibly damaging the surface. First of all, the decrease goes beyond the measured reflectivity for the samples
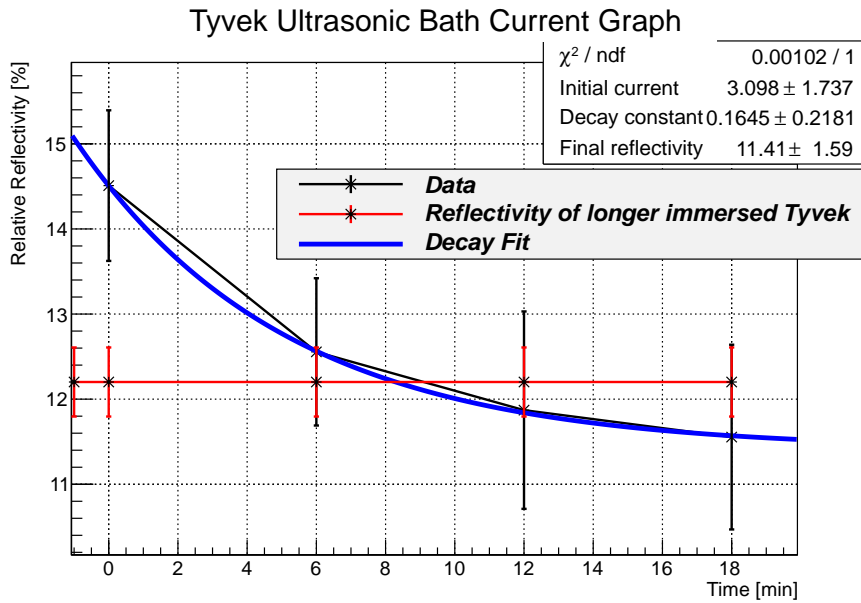
Figure 5.11: The change of *Tyvek* reflectivity after 3 sessions in the ultrasonic bath

left in water over extended periods of time and below the "final reflectivity" from the fit $12.17 \cdot (1 \pm 2.36\,\%)$ %(see figure 5.7, although it does stay within the margin of error of both. The "final reflectivity", which is given by the fit parametre $c = 11.41 \cdot (1 \pm 13.94\,\%)$ % also yields a similar result. In addition, small fibres floated on the water surface after the treatment in the ultrasonic bath and the *Tyvek* seemed more spotted (unfortunately, no photos were taken depicting this).

We cannot conclusively say, whether the ultrasonic bath actually damages the fibres of *Tyvek*, although the aforementioned results and observations certainly indicate this. Since we do not know, whether the value measured for the reflectivity of *Tyvek* immersed in water over an extended period of time (in the order of several days to a few weeks) actually are close to the "final" reflectivity. There is good reason to suspect that the reflectivity does decrease further, as the characteristic time of the "decay" measured in the SD tanks at the PAO (see chapter 2 section 2) is about $1.5$ years.

# Chapter 6

# Measurements of the diffuse and the specular component

It is not only important to quantify to what extent the diffuse and specular component of *Tyvek* differ between used and unsed samples, separately, but also to compare their contribution to the total reflectivity, and what effect immersing the *Tyvek* in water has on this proportion.

The basic idea how to quantify this, is to measure the angular distribution of light reflected off *Tyvek*, namely to measure the signal at different angles of reflection $\theta_r$ for a fixed incident angle $\theta_i$. The implementation is somewhat difficult. Firstly, the setup must be employable in water. Secondly, it is vital to keep the angles stable when changing the sample, in order to allow for a good comparison of the data. Optical fibres guiding the light from a source on the one hand, and as collecting reflected light on the other, can fulfil the former requirement, as they can be immersed in water. Thereby, the angle of incidence and reflection, respectively, can be measured without having take into account the refractive index of water. The way the second problem was solved, was to fix the fibres on a plastic board, which could be lifted when changing the samples, without shifting the position of the fibres with respect to the board. This was done by carving 6 grooves onto its flat side, which radially stretch out from the centre of the long edge, three to the right and three to the left (see figure 6.1). The three grooves of each set are separated by $22.5 \pm 1.5$ degree angles from one another, and are just wide enough to hold a 1 mm optical fibre. This makes it possible to insert the fibres through the grooves and keep them at a steady angle (see figure 6.1), which can be easily determined through geometric measurements. By placing the board standing upright on a sample, with the centre of the long edge, where all the grooves meet, at the bottom, incident light, which is led through through a fibre situated in one of the left set of grooves, can be reflected off the sample's surface, and led through a fibre in one of the right set of grooves into a detector. Thereby, the amount of light reflected at a certain $\theta_r$ can be measured for a fixed $\theta_i$. The angles can be set at $(22.5 \pm 1.5)$ °, $(45.0 \pm 1.5)$ ° and $(67.5 \pm 1.5)$ ° (the board is axially symmetric to the sample surface normal).



Figure 6.1: Plastic board with three grooves of the width of 1 mm optical fibres to the left and the right each, used to measure the angular distribution of light reflected off a *Tyvek* sample

As a light source we used the laser used for the small integrating sphere for the diffuse reflectivity measurements

(see chapter 3 section 2). As a detector we used the same photo diode, coupled to the same amperemetre used in the previous measurements. The "incident fibre" was mounted in such a way that its end extended right to the end of the groove, almost touching the sample. This was done to avoid too large a spread of the light emitted from the fibre. For the "collecting fibre", on the other hand, the end was kept at a slight distance from the sample (1 cm), so that only light channelling through the groove would be collected by the fibre. The schematic of the setup is depicted in figure 6.2. The photo current averaged over 7 positions of the sample (the number of positions had to be reduced in order to be able to measure within a reasonable period of time) was measured for used and unused *Tyvek*, with the measurement error provided by the standard deviation. For calculating the error of the ratio the Gaussian error propagation law was used.
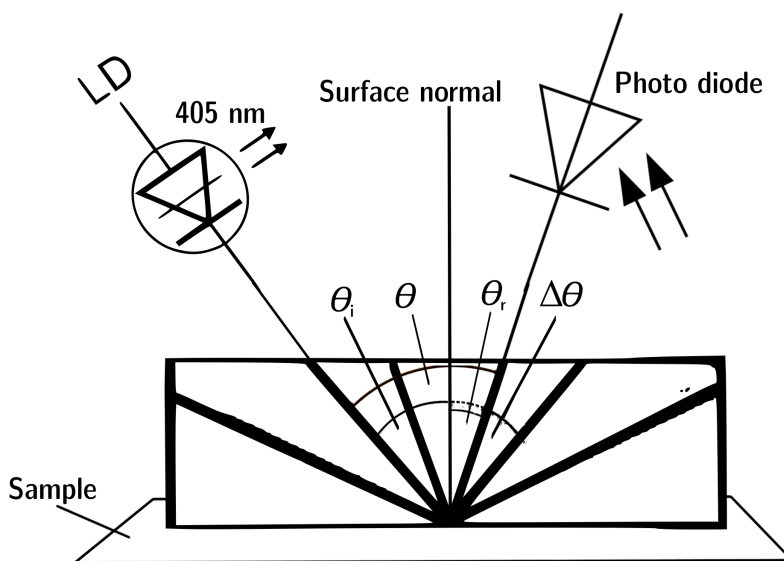


Figure 6.2: Schematic of the setup used to measure the angular distribution of light reflected off the surface of *Tyvek*

**Analysis of data**

The current as a function of the reflection angle for every incident angle in air and in water directly after immersion is plotted in figures A.11 and A.12 for used *Tyvek* and in figures A.13 and A.14 for unused *Tyvek*. The data does not behave as expected from equation 2.1 and from the papers discussed in chapter 2 section 3, as becomes most apparent by the fact that there is no maximum for $\theta_r = \theta_i$. Apparently, there is a high and unknown systematic error involved in changing the grooves, e.g. an altered orientation of the "collecting fibre" resulting in a diverging amount of light collected. Therefore the signal itself cannot be used as a measure of the proportion of the diffuse and specular component, respectively. However, the systematic error should be eliminated by determining the ratio between used and unused *Tyvek*, since the position of the fibres was not changed when exchanging the samples. Thus, the trend of the ratio should give some insight into the different proportions of the diffuse and specular component for each sample, especially considering that unused *Tyvek* has been studied in great detail with the same principle setup (see [14], [15] and [17]). The ratio as a function of the reflection angle in air and in water (both directly after immersion and after several days) in a single graph is plotted for every incident angle in figures 6.3 to 6.5.

For small incident angles (as seen in plot 6.3; $\theta_i = 22.5\,^\circ$) the ratio behaves very similarly in air and in water, with a slightly increased deviation for large angles of reflection ($\theta_r = 67.5\,^\circ$). Given the large measurement uncertainty, one can say that used *Tyvek* and unused *Tyvek* behave similarly with a rising angle of reflection $\theta_r = \theta_i$. For $\theta_i = 45.0\,^\circ$ the same trend is visible for reflection angles up to $\theta_r = 45.0\,^\circ$. After that, the ratio seems to rise sharply for the measurement conducted in air, but I suspect that this is a measurement error, as it actually clearly exceeds 100 %, which is incompatible with the results from chapters 4 and 5, and general expectations. For large incident angles ($\theta_i = 67.5\,^\circ$), the data is very inconclusive, because the ratio again goes well beyond 100 % for $\theta_r = 67.5\,^\circ$, which sheds doubt on the significance of
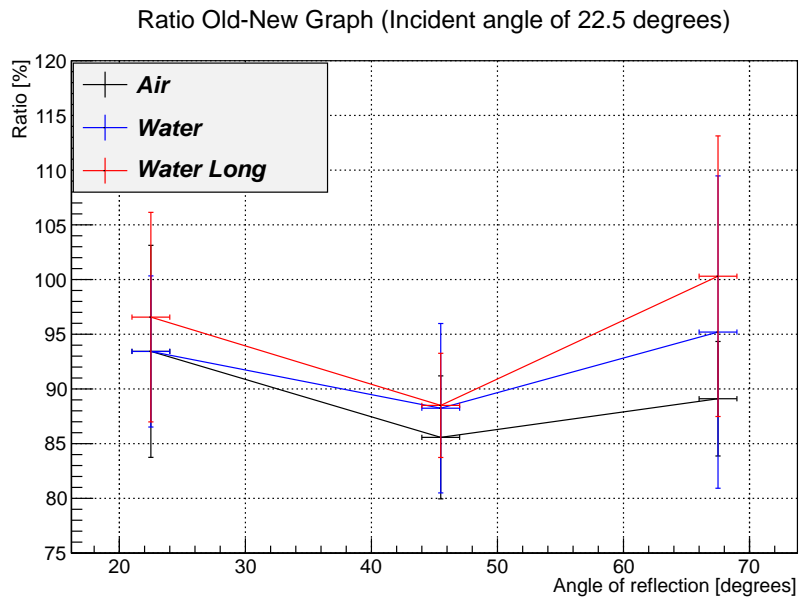
Figure 6.3: The ratio of the spectra of used and unused *Tyvek* in air (black), in water (directly after (blue), and several days after (red), immersion) measured with the above setup for an incident angle of $\theta_i = 22.5\,^\circ$
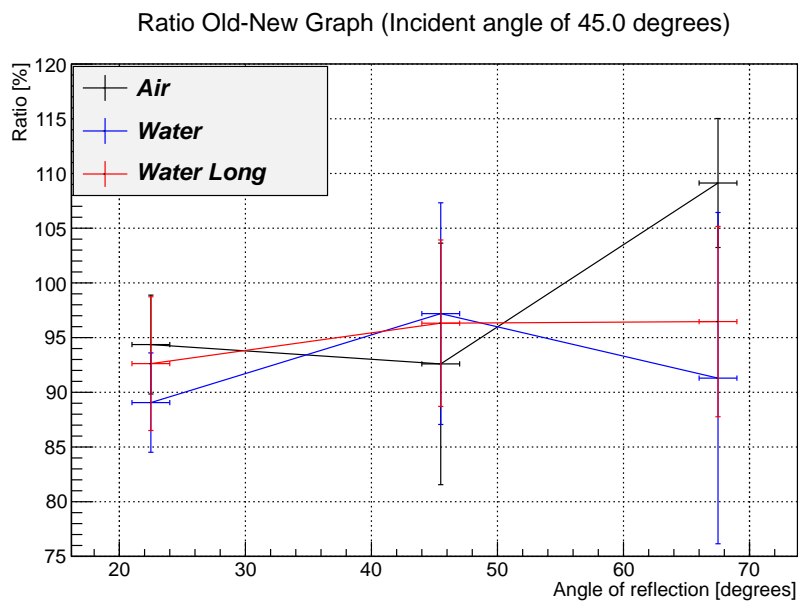


Figure 6.4: The ratio of the spectra of used and unused *Tyvek* in air (black), in water, (directly after (blue), and several days after (red), immersion) measured with the above setup for an incident angle of $\theta_i = 45.0\,^\circ$
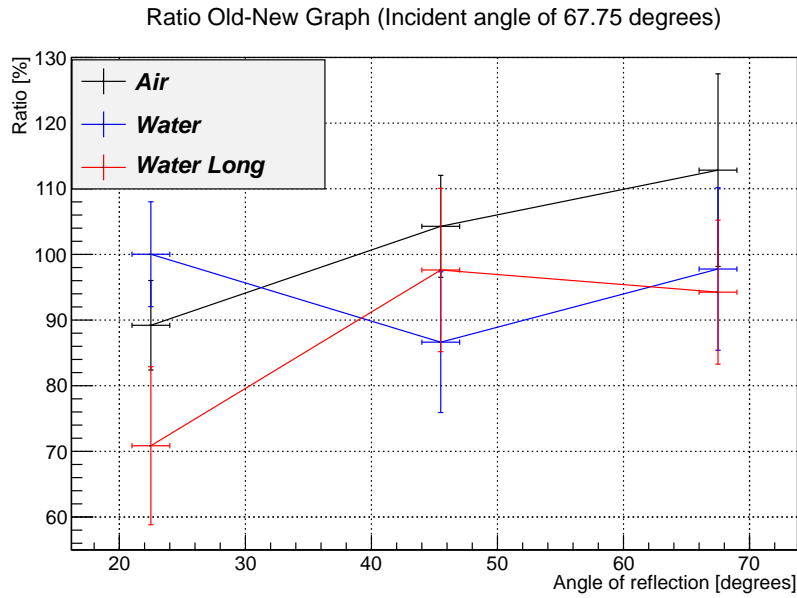
Figure 6.5: The ratio of the spectra of used and unused *Tyvek* in air (black), in water (directly after (blue), and several days after (red), immersion) measured with the above setup for an incident angle of $\theta_i = 67.75\,°$

the remarkably low ratio for the measurement in water after several days at $\theta_r = 22.5\,°$. The remaining data agrees rather well with the above plots, suggesting that the behaviour of used and unused *Tyvek* is actually relatively similar even for large incident angles.

To further test these findings, I also plotted the ratio as a function of the total angle $\theta = \theta_i + \theta_r$, and as a function of the difference of the incident and reflection angle $\Delta\theta = \theta_i - \theta_r$. Of special interest are those ratios, where $\theta$ and $\Delta\theta$ are equal, but have different incident angles. If the above results are true, then one should expect to see the similar values and trends for the ratios for exactly these angles. They can be seen in figures 6.6 and 6.7 for the measurements performed in air, in 6.8 and 6.9 for the measurements performed in water directly after immersion, and in 6.10 and 6.11 for the measurements performed in water several days after immersion.

Apart from the irregularities, which can mainly be attributed to measurement errors, such as ratios larger than 100 % in plots 6.6 and 6.7, or low ratios of around 70 % in plots 6.10 and 6.11, (either these ratios stem from incident angles of $\theta_i = 67.75\,°$, which −, as we already saw −, yielded inconclusive data, or can be discarded , simply by being too high (see blue line in figure 6.6), the behaviour of the ratios is very similar with varying $\theta$ and $\Delta\theta$ for the different angles of incidence. This confirms the above findings.

For each of $\Delta\theta$ plots a constant polynomial was fitted to the data for giving a measure of the average ratio of used und unused *Tyvek* in air, in water directly after immersion, and in water several days after immersion. The plots together with the fit parametres and the $\chi^2$/NDF are depicted in figures 6.12 to 6.14.

The average ratio in air is higher than in water (($94.7 \pm 2.2$) % versus ($92.0 \pm 2.7$) % directly after immersion and ($92.0 \pm 2.6$) % several days after immersion), in accordance with findings from chapter 4 and 5 section 2. In all plots stays between 90 % and 95 %. The $\chi^2$/NDF values indicate a good agreement between the data and a constant ratio, given the high measurement uncertainties.

Though the measurements show irregularities, which need to be appointed to large systematic uncertainties, we can conclude that used and unused *Tyvek* have similar proportions of the diffuse and specular component. All components of the total reflectivity of the *Tyvek* used in the SDs at the PAO seem to have been affected equally, having been reduced by about $5-10$ %.

## Ratio Old-New Air Graph
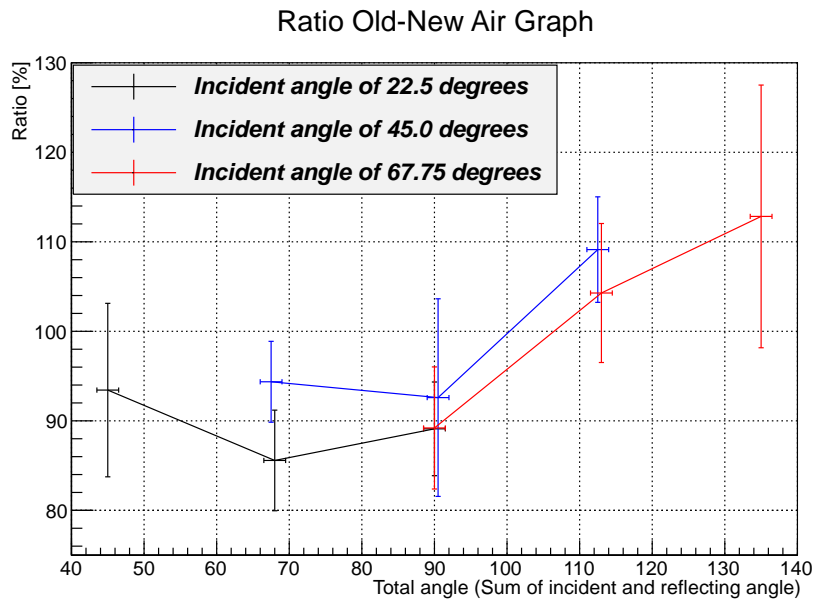


Figure 6.6: The ratio of the spectra of used and unused *Tyvek* in air as a function of the total angle $\theta$; the different incident angles, from which the data was obtained, are marked by colours (black for $\theta_i = 22.5°$, blue for $\theta_i = 45.0°$ red for $\theta_i = 67.75°$)

## Ratio Old-New Air Graph
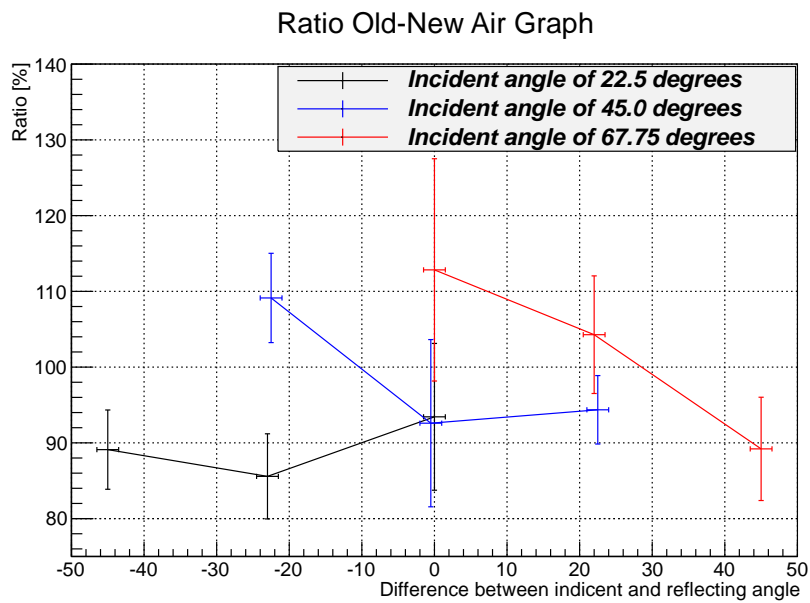


Figure 6.7: The ratio of the spectra of used and unused *Tyvek* in air as a function of the difference between incident and reflection angle $\Delta\theta$; the different incident angles, from which the data was obtained, are marked by colours (black for $\theta_i = 22.5°$, blue for $\theta_i = 45.0°$ red for $\theta_i = 67.75°$)

43
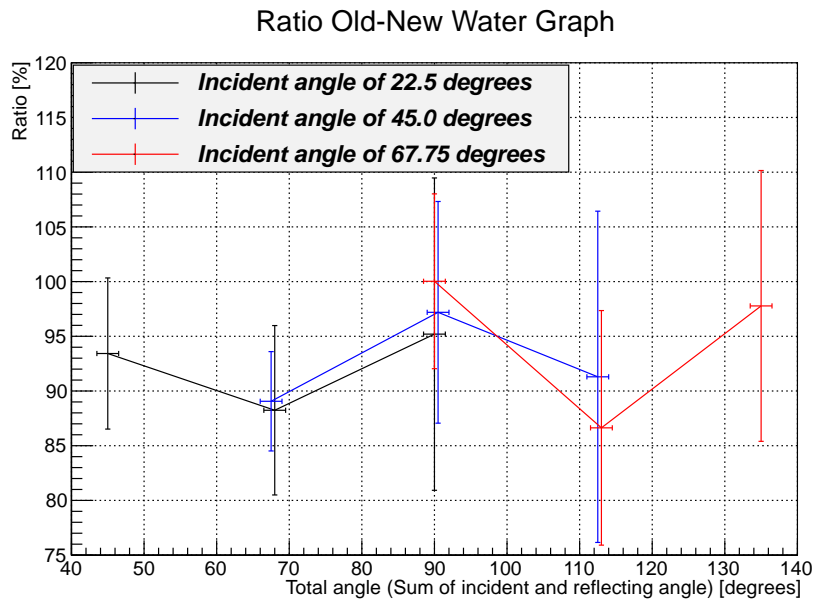
Figure 6.8: The ratio of the spectra of used and unused *Tyvek* in water directly after immersion as a function of the total angle $\theta$; different incident angles, from which the data was obtained, are marked by colours (black for $\theta_i = 22.5\,°$, blue for $\theta_i = 45.0\,°$ red for $\theta_i = 67.75\,°$)
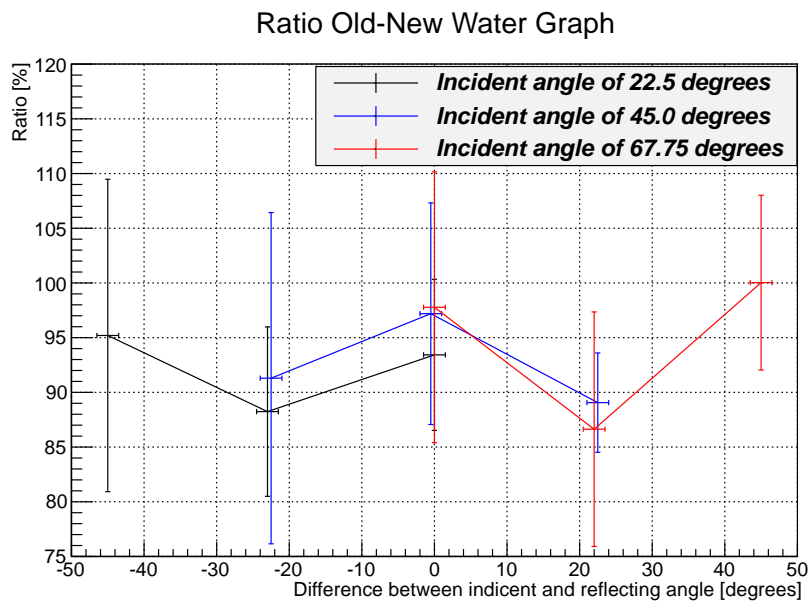


Figure 6.9: The ratio of the spectra of used and unused *Tyvek* in water directly after immersion as a function of the difference between incident and reflection angle $\Delta\theta$; different incident angles, from which the data was obtained, are marked by colours (black for $\theta_i = 22.5\,°$, blue for $\theta_i = 45.0\,°$ red for $\theta_i = 67.75\,°$)
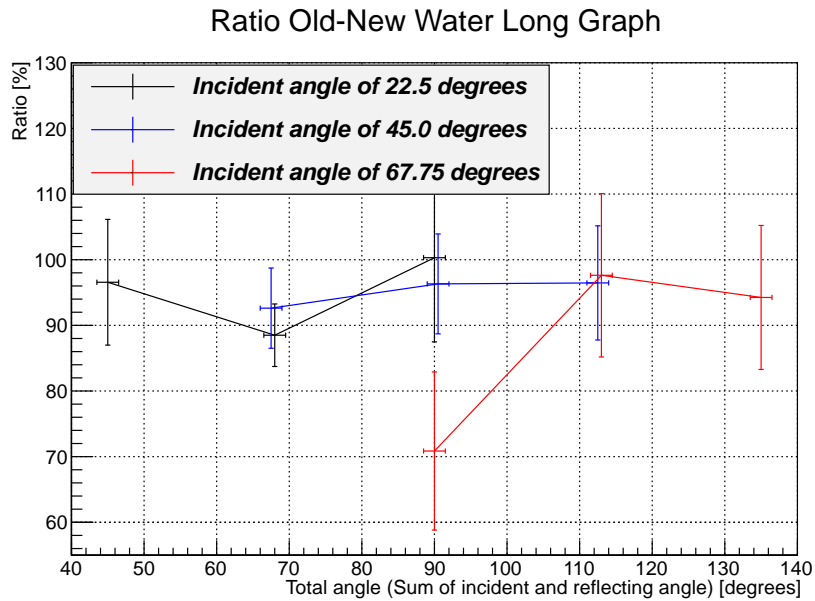
Figure 6.10: The ratio of the spectra of used and unused *Tyvek* in water several days after immersion as a function of the total angle $\theta$; different incident angles, from which the data was obtained, are marked by colours (black for $\theta_i = 22.5$°, blue for $\theta_i = 45.0$° red for $\theta_i = 67.75$°)
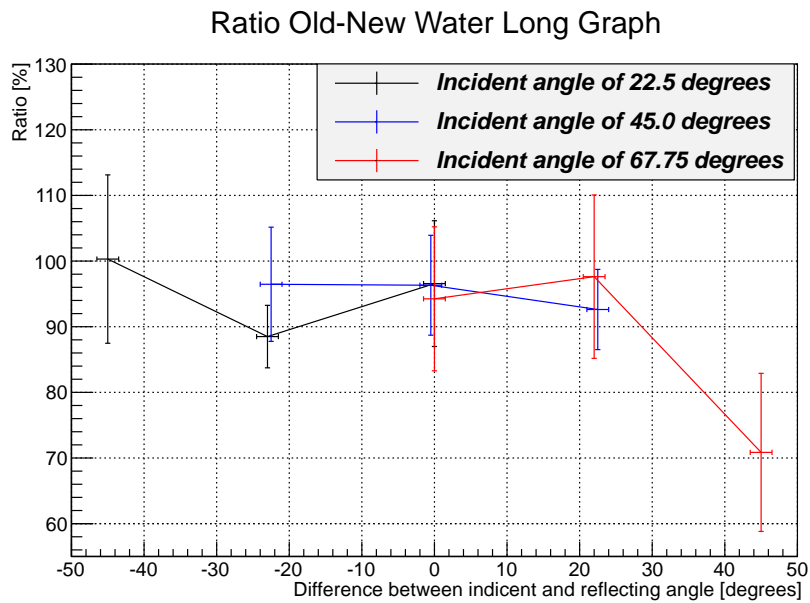


Figure 6.11: The ratio of the spectra of used and unused *Tyvek* in water several days after immersion as a function of the difference between incident and reflection angle $\Delta\theta$; the different incidence, from the data was obtained are marked by colours (black for $\theta_i = 22.5$°, blue for $\theta_i = 45.0$° red for $\theta_i = 67.75$°)
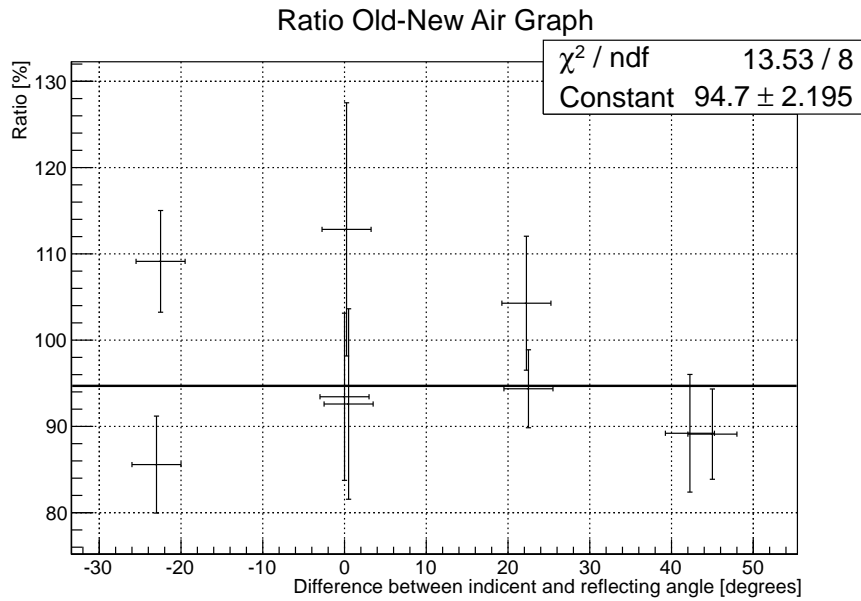
Figure 6.12: The ratio of the spectra of used and unused *Tyvek* in air as a function of the difference between incident and reflection angle $\Delta\theta$; different incident angles were combined into one plot in order to obtain the average ratio
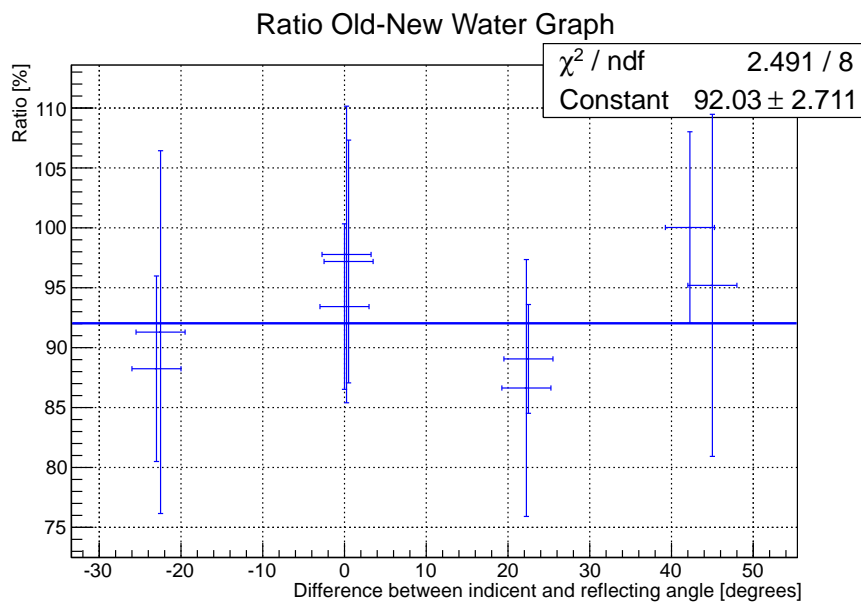


Figure 6.13: The ratio of the spectra of used and unused *Tyvek* in water directly after immersion as a function of the difference between incident and reflection angle $\Delta\theta$; different incident angles were combined into one plot in order to obtain the average ratio
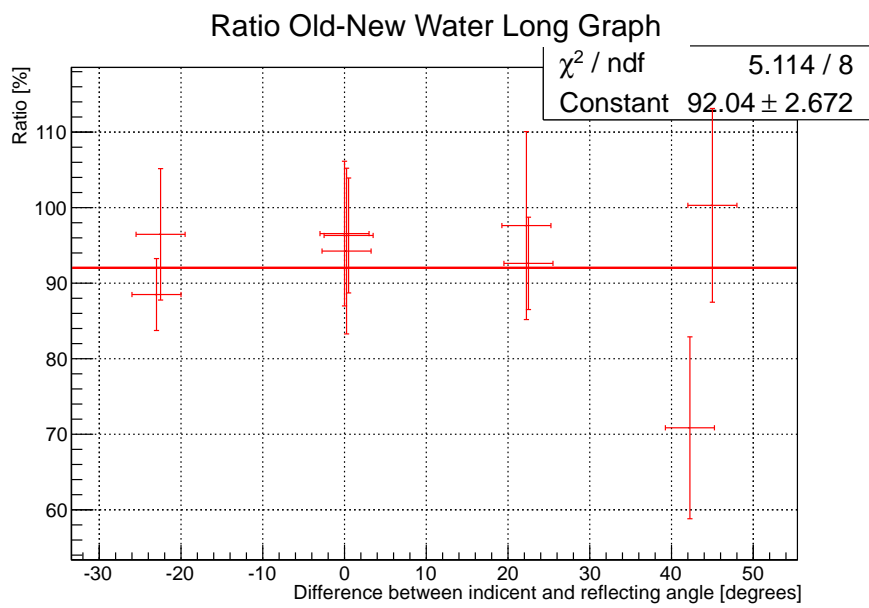
Figure 6.14: The ratio of the spectra of used and unused *Tyvek* in water seeveral days after immersion as a function of the difference between incident and reflection angle $\Delta\theta$; different incident angles were combined into one plot in order to obtain the average ratio

# Chapter 7

# Conclusion

In this thesis, several measurements were performed comparing used and unused *Tyvek* with respect to structure and reflectivity. Although most devices were designed to measure one specific property, they could be used for other properties, as well. I will thus conclude this paper "topicwise" rather than "chapterwise".

In the study of the origins of the observed structural differences between used and unused *Tyvek*, i.e. the black "spots" and the wrinkles in the used sample, SEM scans showed that no microscopic differences are detectable: Both samples had a similar arrangement of fibres, there was, in particular, no discernible abundance of torn fibres in the used sample, nor was it any more contaminated by foreign particles than the unused sample. The used *Tyvek* sample merely had a lower density of fibres in certain regions, and, therefore, a less homogeneous surface overall. A higher inhomogeneity of used *Tyvek* can further be supported by the fact that the reflection measurements with the *reflection probe* had larger scattering when studying used samples. The occurrence of the wrinkles could not be accounted for.

In the diffuse reflection measurements we found that used *Tyvek* has a diffuse reflectivity of up to $3$ % smaller than that of unused *Tyvek*. The difference increases when the samples are immersed in water (up to $10$ %), but so do the measurement uncertainties. The measurement generally shows an uncertainty greater than the value itself, due to the fact that the number of measurements was small, given the available time. The only viable alternative is a larger sphere, which could not be pursued in this thesis. Still, the obtained results are in line with the simulated reflectivity decrease necessary to account for the changing SD tank performance over the years [10].

The results of the specular reflectivity measurements were similar to those for the measurements of the diffuse reflectivity. In air, the difference is about $3$ %, but with a measurement uncertainty of $10$ %. However, due to the consistency of the data, this uncertainty has to viewed as a measure of the inhomogeneity of the surfaces, and the determined difference actually resembling the average difference.

The investigation of the proportions of the diffuse and the specular component, respectively, in the experiment measuring the angular distribution of light reflected off *Tyvek*, showed no measurable differences for used and unused *Tyvek* other than the used sample being smaller by about $5-10$ % than the unused samples. Measurements analysing the effects of varying the distance of the reflection probe head to the sample showed a slightly higher specular component for unused *Tyvek*, but the significance of this result is very limited due to the fact that only a small sample area was measured, and the difference in the probe head height merely differed by $0.1$ mm. In addition, nano bubbles might have emerged in the process of changing the capsules, which would have lead to an increase in the specular component; in light of this fact the measurement would be a measure of the the fibre density rather than of the contribution of the diffuse and specular components; the higher specular component of unused *Tyvek* would imply a higher overall fibre density, which is also in agreement with expectations.

The study of the effects of freezing *Tyvek* revealed no measurable effects, from which follows that freezing, in and of itself, does not affect it reflective properties. The observed decrease of the AoP ratio after the water in the SDs froze, thus, stem from effects which turn up for the given conditions within the tank, e.g. a higher pressure on the walls due to expanding water or ice within the confined volume.

Furthermore, evidence of the existence of nano bubbles in recently immersed *Tyvek* has been found: A similar exponential behaviour of the specular reflectivity with the time of it being immersed in water was measured for both used and unused samples. In addition, treating *Tyvek* in an ultrasonic bath also caused an exponential decrease of its reflectivity. Yet, some observations indicate that the ultrasonic bath damages the fibres of the *Tyvek* in addition to removing nano bubbles (if existent).

In conclusion, the measurements conducted gave some new insight into the differences in the properties between used an unused *Tyvek*. However, many of them were burdened with high measurement uncertainties, so the obtained results are limited in their significance. Certain measurements can be modified to reduce uncertainties: A larger integrating sphere with *Tyvek* walls could be built to measure the diffuse reflectivity, allowing for larger samples sizes, the dependence on the probe head distance to the sample could be performed over a larger area, yielding more representative results, and the angular distribution measurements could be conducted with significantly reduced systematic uncertainties, as has been done in many previous papers (see [14], [15], [16] and [17]).

# Appendix A

# Appendix
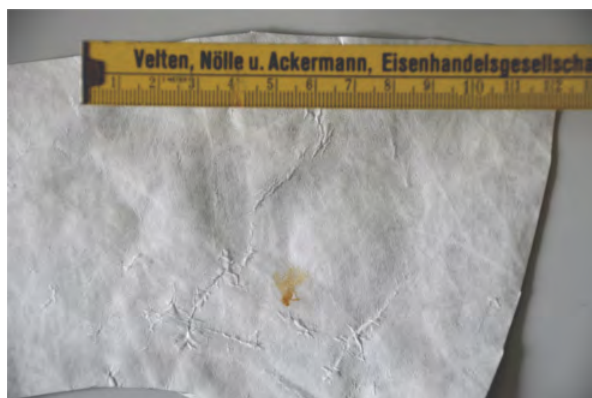


Figure A.1: Photograph of a used sample of *Tyvek* which illustrates both the black "spots" and wrinkles which were observed



Figure A.2: Photograph of deuterium-tungsten light source used for intergrating sphere measurements
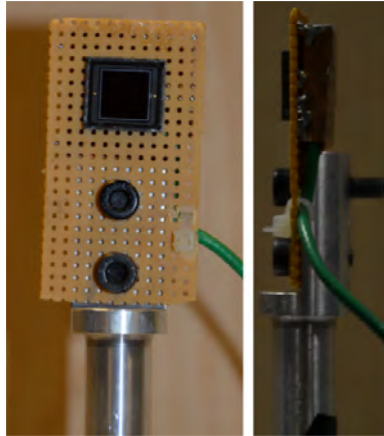
Figure A.3: Front and side view photograph of the photo diode used for measuring the radiant intensity of light



Figure A.4: Photograph of the amperemetre used for measuring the photo current
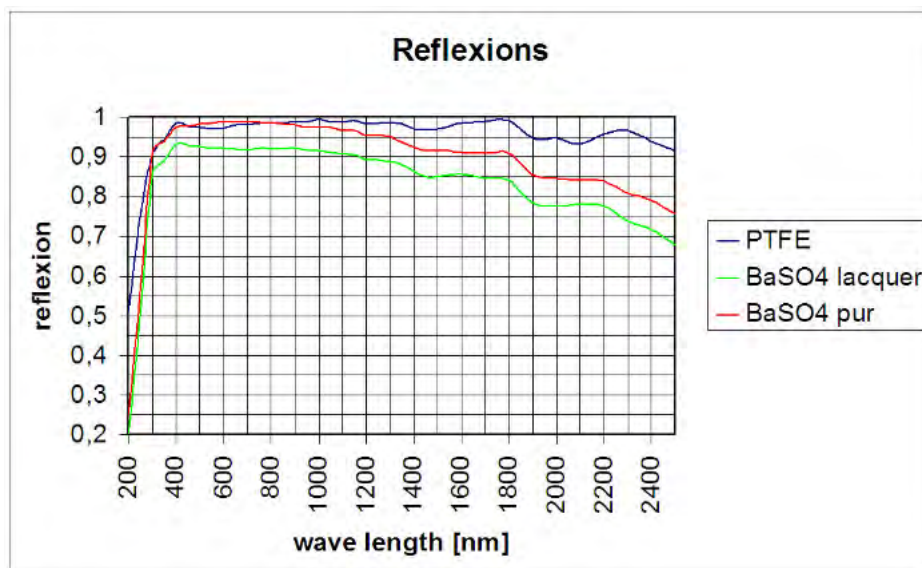


Figure A.5: Absolute reflectivity of $BaSu_4$ as a function of wavlength. The red curve corresponds to the coating used for the "test sphere"

Figure A.6: Photograph of the laser diode used as light source introduced in the diffuse reflectivity measurements in chapter 4 section 2
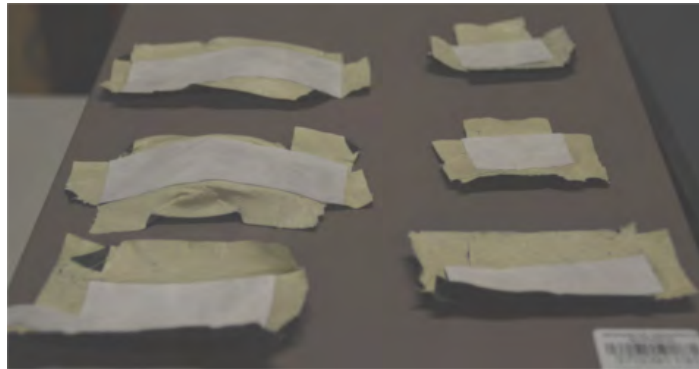


Figure A.7: Photograph of the cut out *Tyvek* samples for the diffuse reflectivity measurements in chapter 4 section 2; the left ones are used samples, while the right ones are unused samples
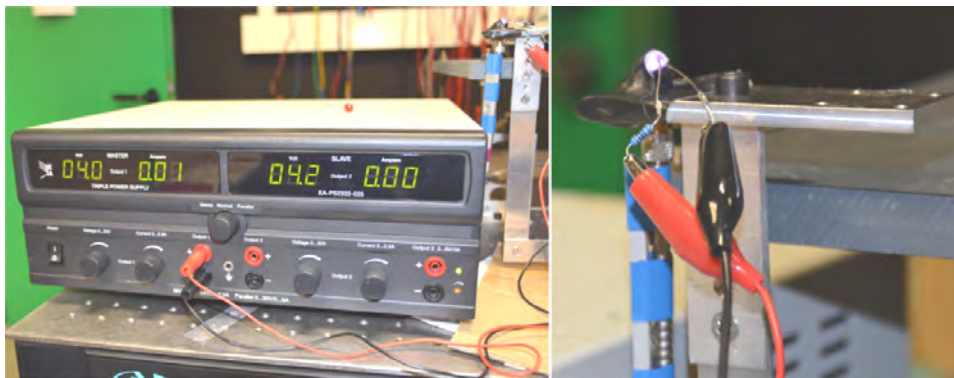


Figure A.8: Photograph of the LED (type G04-187) and its power source set at $4.0$ V
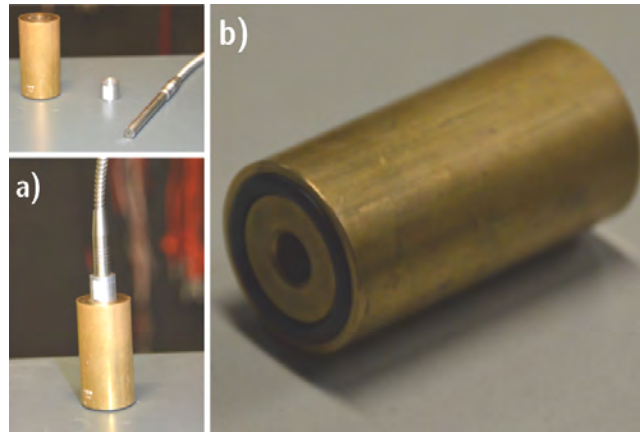
Figure A.9: a) Photographs of the cylinder, in which the probe head can be places; note that an additional "capsule" is needed for the head not to touch the sample surface; b) Photograph of the rubber ring, which keeps the cylinder and thus the probe head fixed

Table A.1: Relative reflectivities (normalised to the calibration mirror) of *Tyvek* in air and water (both directly after immersion and after 5 and 9 days, respectively)

| Measurement medium | Sample | Relative reflectivity |
|---|---|---|
| Air | Unused *Tyvek* | $20.67 \cdot (1 \pm 5.22\,\%)\,\%$ |
| | Used *Tyvek* | $20.09 \cdot (1 \pm 8.88\,\%)\,\%$ |
| Water (directly after immersion) | Unused *Tyvek* | $14.61 \cdot (1 \pm 16.63\,\%)\,\%$ |
| | Used *Tyvek* | $13.11 \cdot (1 \pm 7.21\,\%)\,\%$ |
| Water (after 5 days) | Unused *Tyvek* | $12.20 \cdot (1 \pm 3.40\,\%)\,\%$ |
| | Used *Tyvek* | $11.83 \cdot (1 \pm 8.07\,\%)\,\%$ |
| Water (after 9 days) | Unused *Tyvek* | $12.20 \cdot (1 \pm 3.21\,\%)\,\%$ |
| | Used *Tyvek* | $12.06 \cdot (1 \pm 7.59\,\%)\,\%$ |

Table A.2: Relative reflectivities (normalised to the calibration mirror) of frozen *Tyvek* in air and water

| Measurement medium | Relative reflectivity (before freezing) | Relative reflectivity (after freezing) |
|---|---|---|
| Air (bent) | $20.56 \cdot (1 \pm 6.43\,\%)\,\%$ | $19.93 \cdot (1 \pm 6.32\,\%)\,\%$ |
| Water | $19.94 \cdot (1 \pm 6.28\,\%)\,\%$ | $21.29 \cdot (1 \pm 8.56\,\%)\,\%$ |

Table A.3: Relative reflectivities (normalised to the calibration mirror) of frozen *Tyvek* in air (bent und straight) and water

| Measurement medium | Relative reflectivity (before freezing) | Relative reflectivity (after freezing) |
|---|---|---|
| Air (bent) | $19.99 \cdot (1 \pm 7.14\,\%)\,\%$ | $20.47 \cdot (1 \pm 5.17\,\%)\,\%$ |
| Air (straight) | $19.10 \cdot (1 \pm 6.87\,\%)\,\%$ | $20.83 \cdot (1 \pm 8.85\,\%)\,\%$ |
| Water | $20.08 \cdot (1 \pm 9.83\,\%)\,\%$ | $23.74 \cdot (1 \pm 10.42\,\%)\,\%$ |



Figure A.10: Photograph of the capsules used to vary the distance of the probe head to the sample in chapter 5 section 2.4
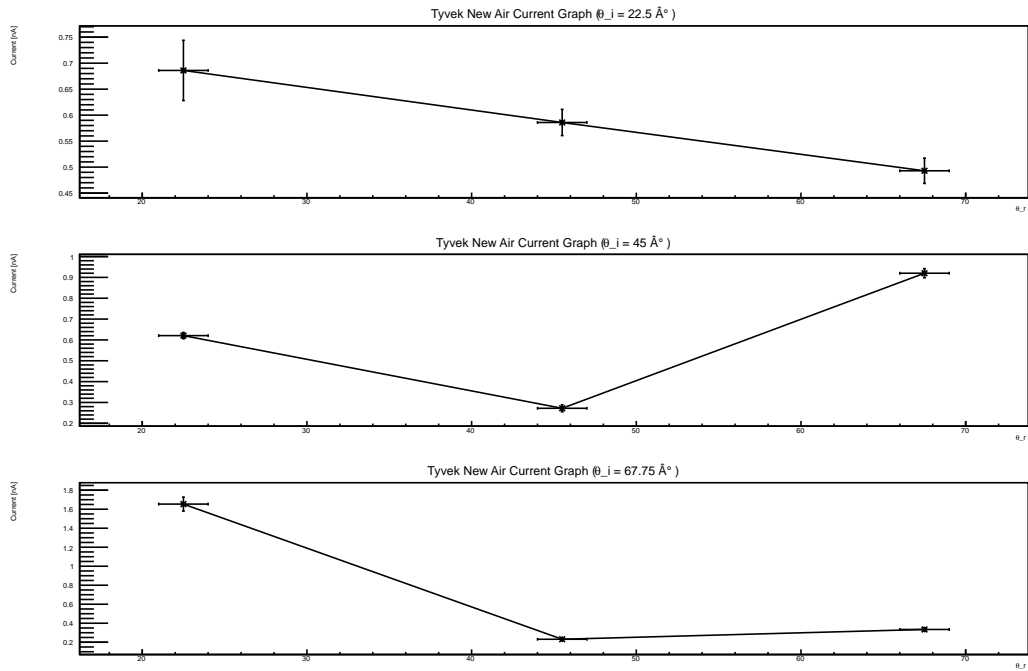
Figure A.11: The angular distribution of light reflect of unused *Tyvek* in air as measured with the setup depicted in 6.2
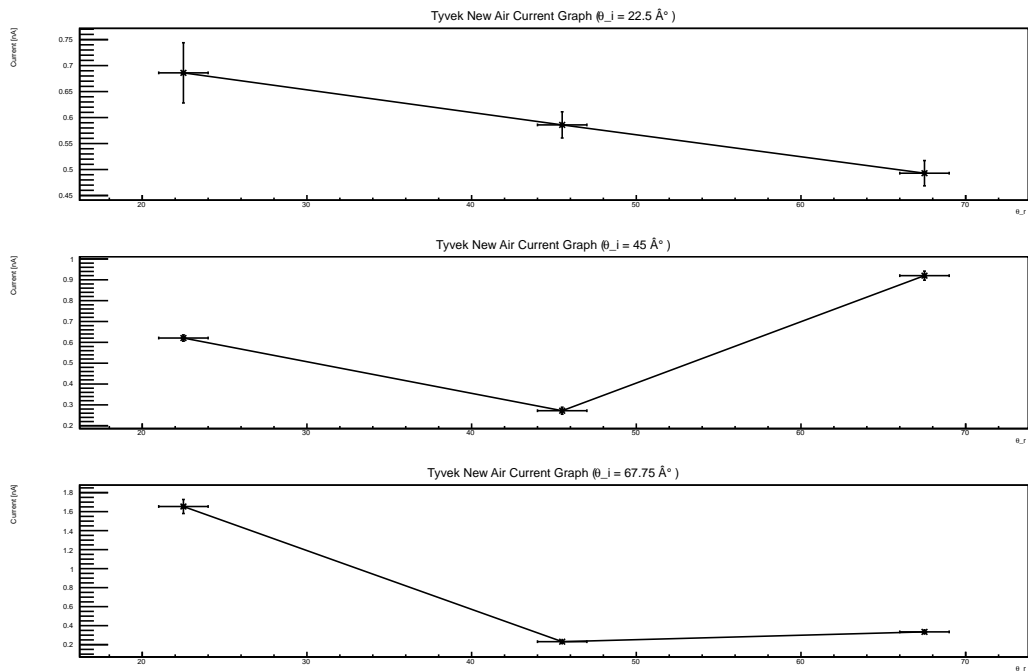


Figure A.12: The angular distribution of light reflect of unused *Tyvek* in water as measured with the setup depicted in 6.2
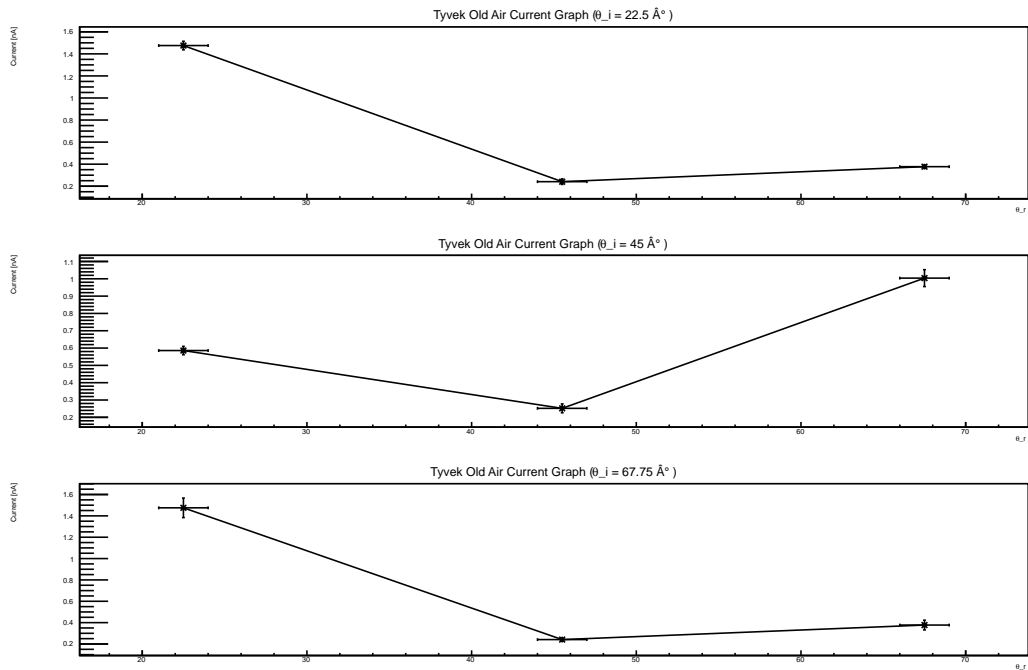
Figure A.13: The angular distribution of light reflect of used *Tyvek* in air as measured with the setup depicted in 6.2
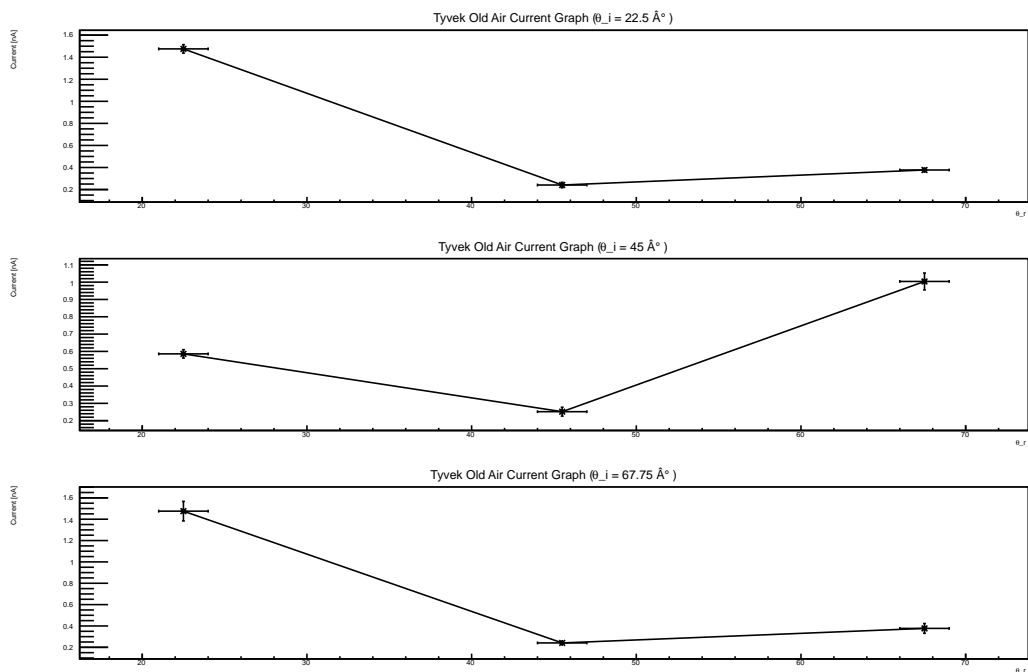


Figure A.14: The angular distribution of light reflect of used *Tyvek* in water as measured with the above setup

# Appendix B

# Bibliography

[1] K.-H. Kampert. Das Pierre Auger Observatorium − Für Teilchenstrahlungen aus dem Kosmos *Technikforum*. Wuppertal, 2012. 1

[2] *http://www2.dupont.com/Tyvek/en_US*. Last accessed: 15.07.2013. 1, 2.3

[3] Claus Grupen. *Astroparticle Physics*. Berlin, Heidelberg: Springer-Verlag, 2005. 2.1, 2.1

[4] *visitantes.auger.org.ar*. Last accessed: 15.07.2013. 2.2

[5] J. Abraham, et al. Properties and performance of the prototype instrument for the Pierre Auger Observatory *Nuclear Instruments and Methods in Physics Research* A 586 (2008) 409–420. http://www.auger.org/reports/ea_nim_2003.pdf. 2.3

[6] I. Allekotte, et al. The surface detector system of the Pierre Auger Observatory *Nuclear Instruments and Methods in Physics Research* A 586 (2008) 409–420. 2.2, 2.4

[7] X. Bertou, et al. Calibration of the surface array of the Pierre Auger Observatory *Nuclear Instruments and Methods in Physics Research* A 568 (2006) 839–846. http://www.ung.si/public/pao/bibl/nim_2006_psa.pdf. Last accessed: 15.07.2013. 2.2, 2.2, 2.2, 2.6

[8] M. Healey, et al. Observation of the Long Term Stability of Water Tanks in the Pierre Auger Surface Detector *GAP NOTE* A 545 (2008) 602–612. 2.2, 2.5, 2.2, 2.7

[9] A. Etchegoyen, et al. Muon-track studies in a water Cherenkov detector *Nuclear Instruments and Methods in Physics Research* 2005-028. http://www.auger.org/admin-cgi-bin/woda/gap_notes.pl. 2.2, 2.2

[10] P. Billoir. *Multi-ageing*. Presentation for Auger Meeting in Lisbon, June 2013 http://indico.nucleares.unam.mx/getFile.py/access?contribId=2&resId=0&materialId=slides&confId=737. Last accessed: 15.07.2013. 2.2, 2.2, 2.8, 7

[11] P. Billoir. *Do the VEM calibration and the attenuation curve age?* LPNHE Paris, February 2013. 2.2, 2.2

[12] H. Wahlberg. Long Term Evolution of the VEM Area to Peak ratio *GAP NOTE* 2012-154. http://www.auger.org/admin-cgi-bin/woda/gap_notes.pl. 2.2, 2.2

[13] H. Wahlberg, R. Sato. Description of the SD freezing events at winters of 2007 and 2010 *GAP NOTE* 2013-041. http://www.auger.org/admin-cgi-bin/woda/gap_notes.pl. 2.2, 2.2, 2.9

[14] A. Filevich et al. Spectral-directional reflectivity of Tyvek immersed in water *GAP NOTE* 1997-065. http://www.auger.org/admin-cgi-bin/woda/gap_notes.pl. 2.1, 2.3, 6, 7

[15] J.C. Arteaga Velazquez et al. Spectral-directional reflectivity of Tyvek immersed in water *GAP NOTE* 2000-035. http://www.auger.org/admin-cgi-bin/woda/gap_notes.pl. 2.3, 6, 7

[16] W. Ling-Yu et al. Study of Tyvek reflectivity in water *Chinese Physics C* Vol. 36, No. 7, Jul., 2012. 2.3, 2.2, 2.3, 2.10, 7

[17] A. Chavarria. *A study on the reflective properties of Tyvek in air and underwater.* Bachelor Thesis. Duke University, 2007. 2.3, 6, 7

[18] Labsphere®, A Halma Company. *Integrating Sphere Theory and Applications.* North Sutton, USA. 2.4, 2.11

[19] S. Reinecke. *Charakterisierung von Spiegeln für den RICH-Detektor von CBM.* Wuppertal, 2011 http://astro. uni-wuppertal.de/html/Theses/Reinecke-Diplom.pdf. 5, 5.3

# Eidesstattliche Erklärung

Hiermit versichere ich, die vorliegende Arbeit selbstständig und unter ausschließlicher Verwendung der angegebenen Literatur und Hilfsmittel erstellt zu haben.

Die Arbeit wurde bisher in gleicher oder ähnlicher Form keiner anderen Prüfungsbehörde vorgelegt und auch nicht veröffentlicht.

Wuppertal, den _____ 

_____
Unterschrift